Draft version April 29, 2019
Typeset using LaTeX **twocolumn** style in AASTeX62

The Rise and Fall of the King: The Correlation between FO Aquarii's Low States and the White Dwarf's Spindown

Colin Littlefield,[1] Peter Garnavich,[1] Mark R. Kennedy,[2] Joseph Patterson,[3] Jonathan Kemp,[4,5] Robert A. Stiller,[1] Franz-Josef Hambsch,[6,7,8,9] Teófilo Arranz Heras,[6,10] Gordon Myers,[6,11,12] Geoffrey Stone,[6,13] George Sjöberg,[6,14] Shawn Dvorak,[6,15] Peter Nelson,[6,16] Velimir Popov,[6,17,18] Michel Bonnardeau,[19] Tonny Vanmunster,[6,7,20,21] Enrique de Miguel,[22,23] Kevin B. Alton,[6,24] Barbara Harris,[6,25] Lewis M. Cook,[6,26] Keith A. Graham,[6,27] Stephen M. Brincat,[6,28] David J. Lane,[6,29] James Foster,[6] Roger Pickard,[30] Richard Sabo,[6,31] Brad Vietje,[6,32] Damien Lemay,[6,33] John Briol,[6,34] Nathan Krumm,[6] Michelle Dadighat,[6,35] William Goff,[6] Rob Solomon,[6] Stefano Padovan,[6] Greg Bolt,[6,36] Emmanuel Kardasis,[6,37] André Debackère,[6,38] Jeff Thrush,[6,39] William Stein,[6,40] Bradley Walter,[6,41] Daniel Coulter,[42] Valery Tsehmeystrenko,[6,43] Jean-François Gout,[6] Pablo Lewin,[6,44] Charles Galdies,[6,45] David Cejudo Fernandez,[6,46] Gary Walker,[6,47] James Boardman Jr.,[6,48] and Emil Pellett[6,49,50]

[1] *Department of Physics, University of Notre Dame, Notre Dame, IN 46556, USA*
[2] *Jodrell Bank Centre for Astrophysics, School of Physics and Astronomy, The University of Manchester, Manchester M13 9P, UK*
[3] *Department of Astronomy, Columbia University, 550 West 120th Street, New York, NY 10027, USA*
[4] *Mittelman Observatory, Middlebury College, Middlebury, VT 05753, USA*
[5] *Visiting Astronomer, Cerro Tololo Inter-American Observatory*
[6] *AAVSO observer*
[7] *Vereniging Voor Sterrenkunde (VVS), Brugge, Belgium*
[8] *Bundesdeutsche Arbeitsgemeinschaft für Veränderliche Sterne e.V. (BAV), Berlin, Germany*
[9] *CBA Mol, Belgium*
[10] *Observatorio Las Pegueras de Navas de Oro (Segovia), Spain*
[11] *Center for Backyard Astrophysics, San Mateo*
[12] *5 Inverness Way, Hillsborough, CA, USA*
[13] *CBA-Sierras, Auberry, CA*
[14] *The George-Elma Observatory, Mayhill New Mexico, USA*
[15] *Rolling Hill Observatory, Lake County, Florida, USA*
[16] *Ellinbank Observatory, Australia*
[17] *IRIDA Observatory, NAO Rozhen, Bulgaria*
[18] *Department of Physics and Astronomy, Shumen University, Bulgaria*
[19] *MBCAA Observatory, Le Pavillon, 38930 Lalley, France*
[20] *CBA Belgium Observatory, Walhostraat 1A, B-3401 Landen, Belgium*
[21] *CBA Extremadura Observatory, 06340 Fregenal de la Sierra, Badajoz, Spain*
[22] *Departamento de Ciencias Integradas, Facultad de Ciencias Experimentales, Universidad de Huelva, E-21070 Huelva, Spain*
[23] *CBA Huelva, Observatorio del CIECEM, Parque Dunar, Matalascañas, E-21760 Almonte, Huelva, Spain*
[24] *Desert Bloom Observatory, Benson AZ, USA*
[25] *Bar J Observatory, New Smyrna Beach, FL*
[26] *CBA Concord, Concord, CA, USA*
[27] *Observatory in Manhattan, IL*
[28] *Flarestar Observatory, San Gwann SGN 3160, Malta*
[29] *Astronomy and Physics, Saint Mary's University, 923 Robie Street, Halifax, NS B3H 3C3 Canada*
[30] *British Astronomical Association Variable Star Section*
[31] *Pine Butte Observatory, Bozeman, Montana*
[32] *Northeast Kingdom Astronomy Foundation, Peacham, VT, USA*
[33] *CBA Quebec, Canada*
[34] *Spirit Marsh Observatory*
[35] *Moka Observatory*
[36] *CBA Perth, 295 Camberwarra Drive, Craigie, Western Australia 6025, Australia*
[37] *Hellenic Amateur Astronomy Association*
[38] *3 FT user (LCO robotic telescope networks)*
[39] *Thrush Observatory, Manchester, MI, USA*
[40] *CBA Las Cruces, Las Cruces, NM, USA*
[41] *Central Texas Astronomical Society*

[42] *Department of Physics and Astronomy, Michigan State University, East Lansing, MI, USA*
[43] *Heavenly Owl Observatory, Odessa, Ukraine*
[44] *The Maury Lewin Astronomical Observatory, Glendora, CA, USA*
[45] *Znith Observatory, Armonie, E. Bradford Street, Naxxar NXR 2217, Malta*
[46] *El Gallinero (El Berrueco, Spain)*
[47] *Maria Mitchell Observatory, Nantucket, MA 02554, USA*
[48] *Krazy Kritters Observatory, 65027 Howath Rd, De Soto, WI, 54624, USA*
[49] *James Madison Memorial High School, Madison, WI, USA*
[50] *Yerkes Observatory, Williams Bay, WI 53191*

ABSTRACT

The intermediate polar FO Aquarii experienced its first-reported low-accretion states in 2016, 2017, and 2018. We establish that these low states occurred shortly after the system's white dwarf (WD) began spinning down, after having spent a quarter-century spinning up. FO Aquarii is the only intermediate polar whose period derivative has undergone a sign change, and it has now done so twice. By combining our spin-pulse timings with previous data, we determine that the WD's spin period has varied quasi-sinusoidally since the system's discovery, and an extrapolation predicts that the white dwarf was spinning down during newly discovered low states in photographic plates from 1964, 1965, and 1974. Thus, FO Aquarii's low states appear to occur exclusively during epochs of spindown. Additionally, our time-series photometry of the 2016-18 low states reveals that the mode of accretion is extremely sensitive to the accretion rate; when the system is fainter than V$\sim$14.0, the accretion onto the WD is largely stream-fed, but when it is brighter, it is almost exclusively disk-fed. The system's grazing eclipse remained detectable throughout all observations, confirming the uninterrupted presence of a disk-like structure, regardless of the accretion state. Our observations are consistent with theoretical predictions that during the low states, the accretion disk dissipates into a ring of diamagnetic blobs. Finally, a new *XMM-Newton* observation from 2017 indicates that the system's anomalously soft X-ray spectrum and diminished X-ray luminosity in the wake of the 2016 low state appear to be long-lasting changes compared to pre-2016 observations.

Keywords: stars:individual (FO Aquarii, FO Aqr); novae, cataclysmic variables; binaries: eclipsing; white dwarfs; accretion, accretion disks; stars: magnetic field

1. INTRODUCTION

Despite its stature as one of the most extensively studied intermediate polars (IPs), FO Aquarii (hereinafter, FO Aqr) continues to offer fresh insight into this class of object, even four decades after its discovery. IPs are a subset of the cataclysmic variable stars (CVs), which are semi-detached binaries with an accreting white dwarf (WD) and a low-mass secondary star. The characteristic that distinguishes IPs from other CVs is the WD's magnetic-field strength, which is high enough to disrupt the accretion flow but low enough that it cannot synchronize the WD rotational period with the binary orbital period (for a review, see Patterson 1994).

While non-magnetic CVs accrete from an accretion disk, IPs can accrete from either a disk or the accretion stream from the companion star, which loses mass due to Roche-lobe overflow. The WD's magnetospheric radius determines the mode of accretion onto the WD; a large magnetosphere will disrupt the accretion stream before it can circularize into a disk, while a small one will allow the formation of a disk whose inner region is truncated at the magnetospheric radius. The former is referred to as stream-fed or 'diskless' accretion, while the latter is generally known as 'disk-fed' accretion. Further complicating matters is the fact that some systems show evidence of simultaneous stream-fed and disk-fed accretion. The prevailing model for these hybrid systems is that although they possess a disk, some of the accretion stream from the donor star is able to overflow the disk and collide with the magnetosphere (Hellier 1993), although accretion from tidally induced disk structure is another possibility (Murray et al. 1999).

Power spectral analysis is one common method of diagnosing the mode of accretion in an IP. At optical wavelengths, disk-fed accretion results in a strong signal at the WD's rotational frequency (ω) because the inner disk is expected to be azimuthally uniform. Stream-fed accretion gives rise to signals at the spin-orbit beat frequency ($\omega - \Omega$), the orbital frequency (Ω), and some-

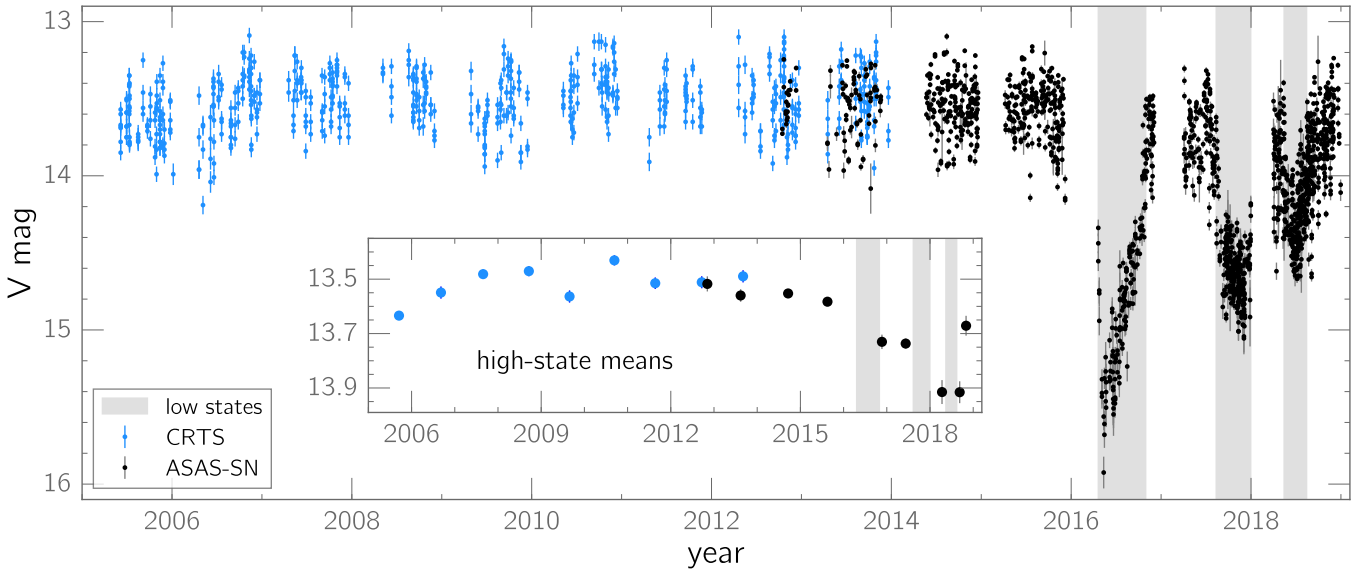

Figure 1. Long-term light curve of FO Aqr derived from observations by CRTS (Drake et al. 2009) and ASAS-SN (Shappee et al. 2014; Kochanek et al. 2017).The scatter is due to FO Aqr's large-amplitude, short-period variability. The inset panel shows the system's mean yearly magnitude outside of the three low states. In 2018, three means are plotted in order to better represent the pre- and post fade behavior. In both panels, CRTS observations are unfiltered with a V zeropoint, while ASAS-SN observations are primarily V-band, with g-band observations interspersed beginning in September of 2017. By comparing the mean magnitude of the system in the three bandpasses during overlapping coverage, we find that the zeropoint offsets are very small in relation to the depth of the low states, so we do not apply a zeropoint correction. Five spurious CRTS measurements have been excised from the unbinned light curve.

times the second harmonic of the the beat frequency, $2(\omega - \Omega)$ (Ferrario & Wickramasinghe 1999).

Irrespective of the accretion mechanism, the WD's magnetic field captures the accretion flow when the magnetic pressure exceeds the internal ram pressure of the flow. As it travels along the magnetic field lines, the gas forms a three-dimensional accretion curtain that corotates with the WD and impacts in an X-ray-emitting shock just above the WD's surface. Depending on the colatitude of the magnetic axis and the orbital inclination, the WD's rotation can cause a periodic variation in the aspect of the accretion curtain as well as regular disappearances of the accretion shock behind the limb of the WD. These effects generate optical and X-ray pulsations, respectively, at the WD's spin frequency (ω). Accurate timing of the spin pulsations can be used to monitor the evolution of the WD's spin period.

A number of CVs have undergone periods of diminished mass transfer. These episodes, during which the diminished accretion rate causes the system to fade by several magnitudes, are widely attributed to the passage of starspots across the secondary star near the L1 point (Livio & Pringle 1994). Low states are especially interesting in IPs because of the possibility that the accretion disk will entirely dissipate once the mass-transfer rate has dropped below a critical threshold (Hameury & Lasota 2017). However, relatively few low states have been observed in IPs, with Swift J0746.3-1608 (Bernardini et al. 2019) being one of the few examples.

1.1. *FO Aqr*

1.1.1. *Overview*

Patterson & Steiner (1983) discovered FO Aqr as the optical counterpart of a previously known X-ray source from Marshall et al. (1979) and concluded that it was an IP. It distinguished itself with a large-amplitude, 21-minute optical pulsation whose exceptional stability led Patterson & Steiner (1983) to nickname FO Aqr "the king of the intermediate polars." The binary has a 4.85-hour orbital period, punctuated by a feeble eclipse. The eclipse is visible in broadband optical photometry but not in X-rays, leading Hellier et al. (1989) to propose that only the outer disk is occulted. The phasing of the eclipse has remained stable for decades (Bonnardeau 2016, and references therein), and while the eclipse waveform is normally overwhelmed by the spin pulses, phase-folded light curves of many orbital cycles suppress the spin contamination and plainly reveal the eclipse (e.g., Kennedy et al. 2016). The distance to FO Aqr is 518^{+14}_{-13} pc, based on a probabilistic inference (Bailer-Jones et al. 2018) from its Gaia DR2 (Gaia Collaboration et al. 2018) parallax of 1.902 ± 0.051 mas.

1.1.2. *Spin period*

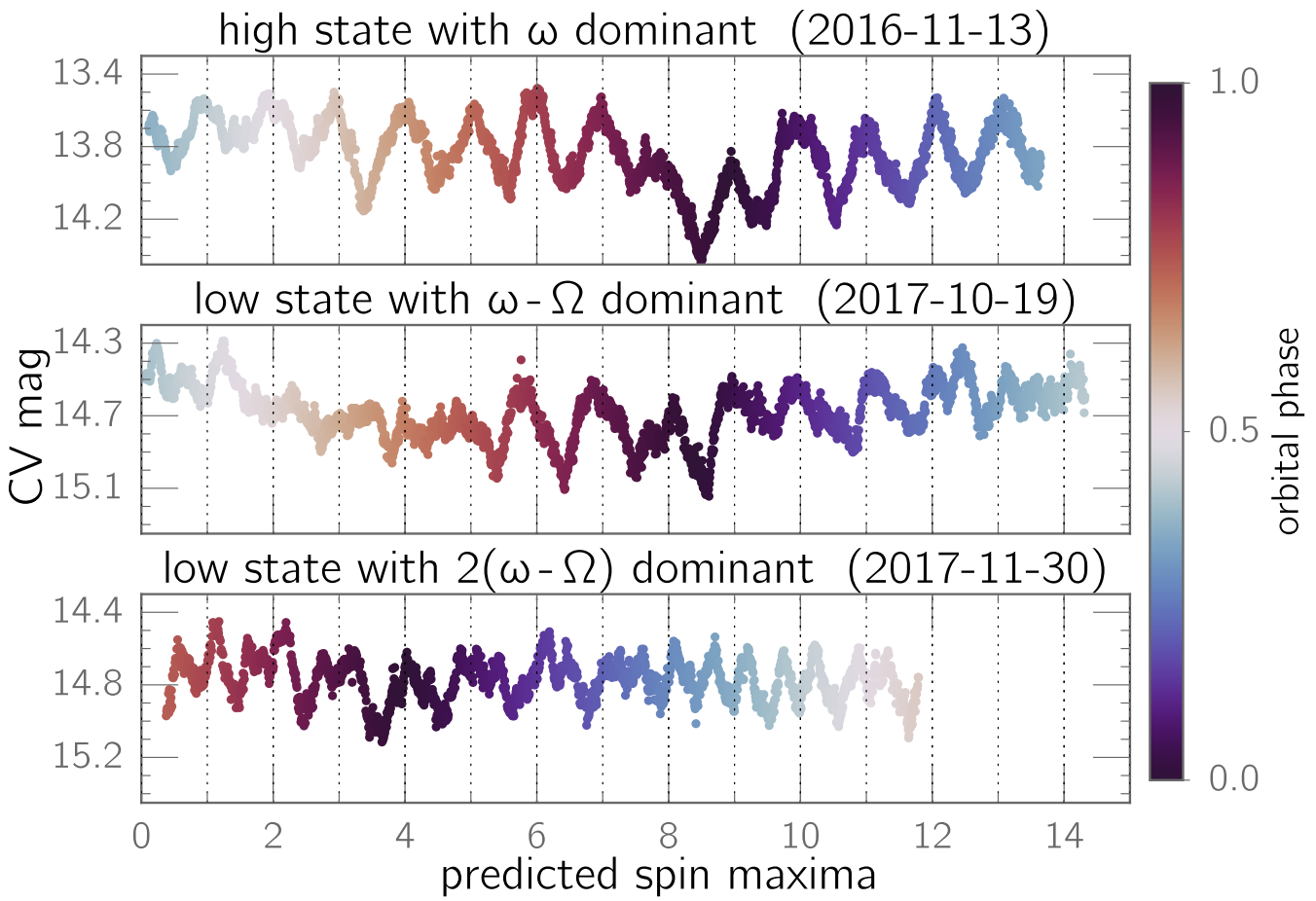

Figure 2. Representative light curves of FO Aqr in different accretion states. The dotted vertical lines indicate the expected times of spin-pulse maxima in each light curve. The vertical and horizontal scales are identical for each light curve, and the color of each point represents the orbital phase of the observation. As noted in Sec. 1.1.3, the relative strengths of the ω, $\omega - \Omega$, and $2(\omega - \Omega)$ frequencies change between the high and low states. The eclipses tend to be difficult to identify in any individual time series.

The spin period of the WD has received extensive attention in the literature, and the ever-increasing baseline of observations has painted a complicated picture of its evolution since the system's discovery.

It took several years after the discovery of FO Aqr to establish a sufficient baseline for Pakull & Beuermann (1987) and Shafter & Macry (1987) to identify a positive $\dot{P}$—*i.e.*, an increasing rotational period of the WD, commonly referred to as a "spin-down." Osborne & Mukai (1989) subsequently measured a significant $\ddot{P}$ term that indicated that the rate of the spin-down was decreasing, and Steiman-Cameron et al. (1989) found that $\dot{P} \approx 0$ in 1987. Around this time, FO Aqr entered an era of spin-up, as described by the cubic ephemerides of the spin maxima from Patterson et al. (1998) and Williams (2003). While Williams (2003) was able to extend his ephemeris to 1998, a cycle-count ambiguity prevented him from identifying a unique ephemeris that incorporated his timing measurements from 2001 and 2002, so he proposed three possible fits to the pulse timings.

Three subsequent papers weighed in on this cycle-count ambiguity. Andronov et al. (2005) measured the spin period in 2004 and found that it implied an extreme spin-up, far in excess of any of the three Williams (2003) fits. Kennedy et al. (2016) found that the spin period during *Kepler K2* observations from 2014-2015 was significantly longer than the Andronov et al. (2005) period and interpreted this as evidence that the system had transitioned back to spin-down. Bonnardeau (2016) proposed a solution to the Williams (2003) cycle-count ambiguity and showed that the O−C residuals from a quadratic ephemeris implied a ∼25-year oscillation. However, no paper has reported an ephemeris to supersede the one from Williams (2003).

In Littlefield et al. (2016, hereinafter, "Paper I"), we muddied the waters by showing an apparent phase shift of the spin pulse in response to the system's luminos-

ity. We speculated that the phase shift could be the result of a change in the accretion geometry but cautioned that it needed to be confirmed. Fortunately, Kennedy et al. (2017) dug deeper into the issue and found that the purported phase shift was attributable to a minuscule inaccuracy in the WD spin period from Kennedy et al. (2016), propagated across two years. Although the period was constant throughout the *K2* observations, there were small phase shifts of the spin pulse in response to the system's overall luminosity, and these shifts caused the Lomb-Scargle periodogram to yield a period that was inaccurate by just a few milliseconds (Kennedy et al. 2017). There are two critical takeaways from Kennedy et al. (2017) about the spin ephemeris: (1) the phase shift from Paper I was not of astrophysical origin and (2) more broadly, modeling a light curve of FO Aqr with a periodic function is not a reliable means of extracting either the time-averaged spin period or the time of one fiducial photometric maximum.

The latter point requires some elaboration. Many previous works have fitted a trigonometric function to an entire season of time-series photometry of FO Aqr and used this model to extract one representative time of photometric maximum, even though the underlying dataset might contain a large number of photometric maxima. However, the effect identified by Kennedy et al. (2017) highlights one mechanism through which subtle variation within a dataset can thwart this type of approach. By comparison, the measurement of individual pulse timings allows a more direct and transparent means of identifying possible systematic errors, such as the correlation between pulse O−C and orbital phase (Osborne & Mukai 1989).

1.1.3. *Low states*

FO Aqr is notable for undergoing deep low states caused by a diminution of the binary's mass-transfer rate. This behavior is a recent development for FO Aqr. Between 1983-2015, its overall optical luminosity remained stable, and an examination of sparsely sampled archival photographic plates obtained between 1923-1953 showed no low states (Garnavich & Szkody 1988); as of the end of 2015, FO Aqr had always been reported in a high state. However, when it emerged from solar conjunction in 2016 April, the system was ∼2 mag fainter than it had been prior to conjunction (Paper I). Additional low states occurred in 2017 (Littlefield et al. 2017) and 2018 (Littlefield et al. 2018). Fig. 1 illustrates the recent spate of low states by plotting the long-term light curve of FO Aqr from the Catalina Real-Time Sky Survey (Drake et al. 2009) and the All-Sky Automated Survey for Supernovae (ASAS-SN; Shappee et al. 2014; Kochanek et al. 2017).

Of this trio of low states, only the 2016 event has been examined in any meaningful detail in the literature. In Paper I, we reported optical time-series photometry of part of the low state, finding that the dominant signal in the optical power spectrum transitioned from ω in the high state to $\omega-\Omega$ and $2(\omega-\Omega)$ in the low state. We interpreted this as evidence of a shift from predominantly disk-fed accretion to a stream-overflow or stream-fed geometry in the low state. We also determined that the eclipse depth and width decreased during the low state. However, since the recovery was still underway when the paper was published, Paper I does not describe the final stages of the low state. X-ray observations of the 2016 low state by Kennedy et al. (2017) provided independent support for a stream-fed accretion geometry and revealed that the spectrum had softened in comparison to archival high-state X-ray observations.

1.1.4. *A note on low-state terminology*

There are no formal definitions for low, intermediate, and high states, so the same terminology can have subtly incongruous meanings in different studies, particularly when comparing observations obtained across the electromagnetic spectrum.

Throughout this paper, we use the terms "low state" and "faint state" interchangeably to describe FO Aqr when it has has faded sufficiently that its optical power spectrum shows modulations at $\omega-\Omega$ and/or $2(\omega-\Omega)$ whose amplitude is comparable to that of the spin frequency ω. If power spectral information is unavailable, as is the case for archival photographic plates, we define a low state as an extended period during which FO Aqr faded below magnitude 14.0 in either the B or V bands; Sec. 7.4 explains the rationale for this particular cutoff. In contrast, when FO Aqr is bright, ω typically overwhelms $\omega-\Omega$ and its harmonics, and we refer to this as a "high state" or a "bright state."

Thus, the "recovery state" described in Kennedy et al. (2017), during which FO Aqr's X-ray luminosity remained significantly less than usual, would be called a high state after applying our criteria to the contemporaneous optical light curve.

2. DATA

2.1. *Optical photometry*

Our dataset consists of time-series photometry of FO Aqr in its 2016, 2017, and 2018 observing seasons, obtained with a variety of instruments. A majority of the time series were obtained by amateur astronomers in response to AAVSO Alert Notices 545, 598, and 644

(Waagen 2016, 2017, 2018, respectively). These data were either V-filtered or unfiltered with a V zeropoint. All told, amateur astronomers contributed a staggering 2,870 hours of time-series photometry across the three observing seasons — over 90% of our time-series data.

We also obtained numerous unfiltered time series in each of the three observing seasons with the University of Notre Dame's 80-cm Sarah L. Krizmanich Telescope (SLKT) at a typical cadence of 8 sec per image.

Fig. 2 plots three representative time series from our dataset: one from a high state and two from low states. The AAVSO, *K2*, ASAS-SN, and CRTS datasets are all freely available for download, while the SLKT and all other photometry can be obtained from either the corresponding author (C.L.) or from the journal website.

To check the internal consistency of the data, we identified overlapping light curves from different observers and checked for temporal or magnitude offsets. We identified observers who had consistent zeropoints and, as necessary, applied constant offsets to reduce zeropoint offsets. These offsets were small—usually only several hundredths of a magnitude.

The fundamental difficulty with measuring FO Aqr's overall brightness is the fact that its light curve is constantly fluctuating, as exemplified by the large scatter in Fig. 1. Because its short-period variability can exceed an amplitude of 0.5 mag over the course of a WD rotational cycle, a single snapshot observation of FO Aqr can yield an inaccurate measurement of FO Aqr's overall brightness, depending on how it samples the spin pulsation. For similar reasons, the orbital modulation, which is poorly defined and shows significant cycle-to-cycle variation, also contaminates snapshot measurements. Further complicating matters is the presence of slow, apparently aperiodic variability of up to several tenths of a magnitude over the course of several days in the high state (Kennedy et al. 2016).

Finding the average brightness across a long time series mitigates these problems, and we used the two-month-long *K2* light curve (Kennedy et al. 2016) to simulate the effectiveness of this technique via Monte Carlo simulations. In each simulation, we randomly selected from the *K2* light curve a segment whose duration was chosen from the uniform domain [20 min, 8 h]. We then calculated both the mean magnitude during this segment and the mean magnitude within a one-day window centered on the midpoint of that segment. We took the difference between these two values to be the error in the overall brightness. We repeated this procedure for 25,000 different segments of the *K2* light curve and found that the 1σ uncertainty in magnitudes is well-described by a decaying exponential of $E(t) = 0.048e^{-3.3t} + 0.029$, where t is the light-curve duration in hours. We used this function to compute uncertainties for the average magnitude from each light curve. Although this approach hinges upon the questionable assumption that the slow, aperiodic variability in the high-state light curve is a reasonable approximation of the corresponding behavior in the low state, we are not aware of a more robust method of realistically estimating the systematic uncertainties.

2.2. *XMM-Newton observations*

DDT observations of FO Aqr were obtained using the *XMM-Newton* satellite for 43 ks on 2017 May 12-13 (Obs. ID 0794580701). The EPIC-pn (Strüder et al. 2001) and EPIC-MOS (Turner et al. 2001) cameras used a medium filter and were operated in the small-window mode. The optical monitor (OM; Mason et al. 2001) observed FO Aqr with the UVW1 filter during the first half of the observing run and with the UVM2 filter during the second half. We analyzed the data using standard routines in the *XMM-Newton* Science Analysis Software (SAS). All photon-arrival times were corrected to the solar system's barycenter using SAS's BARYCEN function.

3. DISCOVERY OF LOW STATES IN DIGITIZED PHOTOGRAPHIC PLATES FROM APPLAUSE

The Harvard plates analyzed in Garnavich & Szkody (1988) were obtained sporadically between 1923-1953, with the coverage being significantly denser during the final 23 years. Since the earliest reported optical photometry was obtained in 1981 (Patterson & Steiner 1983), this leaves a 28-year gap in FO Aqr's observational record. Fortunately, the digitized photographic plates made available through the Archives of Photographic Plates for Astronomical Use (APPLAUSE) project[1] make it possible to explore this previously unexamined period of FO Aqr's history. The B-band light curve from APPLAUSE (Fig. 3) reveals at least two low states during which the system faded to $B \sim 14.7$ in 1966 and 1974. Moreover, in 1965, FO Aqr was consistently observed near $B \sim$14.1, which is a half-magnitude fainter than its brightness in the high-state APPLAUSE light curve.

Unfortunately, the sampling of the low states is insufficiently dense to offer much information beyond a constraint on their depth: $\gtrsim 0.5$ mag in 1965 and $\gtrsim 1$ mag in 1966 and 1974. On a related note, it is unclear whether the 1965 and 1966 low states were part of the same event. While there are no observations of the system in a high

[1] https://www.plate-archive.org/applause/

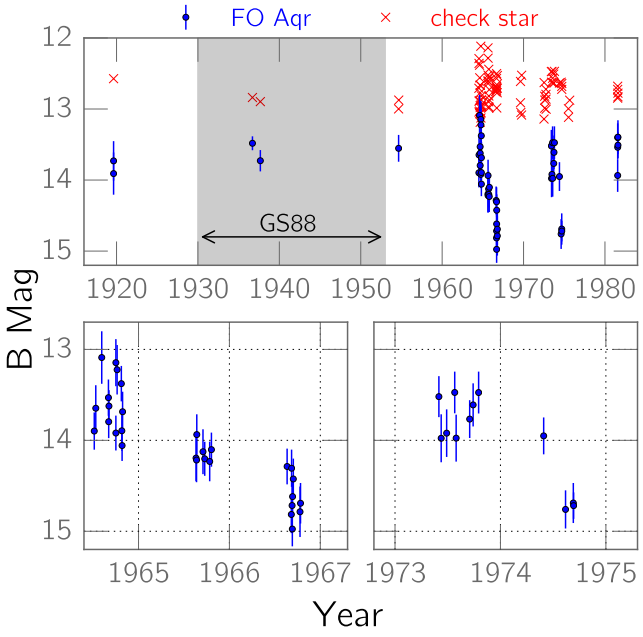

Figure 3. Top: The APPLAUSE light curve of FO Aqr, showing low states in 1965, 1966, and 1974. The check star is UCAC4 409-138165. The shaded gray region indicates a twenty-three year span of intensive coverage in the Harvard plate archive. Garnavich & Szkody (1988) found no low states during that interval. **Bottom left:** Closeup of the 1964-1965 faint states. It is unknown whether the 1965-66 observations were obtained during the same low state or during separate events. **Bottom right:** Closeup of the 1974 faint state.

state between those two low states, this could be due to a lack of observations.

The only two APPLAUSE observations of FO Aqr obtained between 1923-1953 showed FO Aqr in a high state, so there is no contradiction between the APPLAUSE data and the Harvard plates analyzed in Garnavich & Szkody (1988).

4. SPIN EPHEMERIS

4.1. *New ephemeris*

We have calculated a new rotational ephemeris that describes all spin-pulse timings since year 2002.7 without any cycle-count ambiguities. To accomplish this, we took high-state, time-series photometry of FO Aqr from the SLKT dataset, the AAVSO database, the *K2* light curve, and Bonnardeau (2016)[2] and extracted photometric maxima by fitting a fourth-order polynomial to the local light curve around each pulse. The fitting algorithm rejected low-quality timings, such as those caused by inadequate sampling of an individual pulse or a by smeared pulse profile that lacks a clearly defined peak. All told, this dataset contains 5,670 pulse timings, including 4,715 pulse timings from the *K2* light curve, 259 from AAVSO/CBA photometry obtained between 2002-2015, and 314 timings from the Bonnardeau (2016) photometry. Moreover, the combined SLKT / AAVSO dataset obtained during the bright interregnum between the 2016 and 2017 low states (Fig. 1) contained 353 usable pulse timings.

To build the ephemeris, we started by using the linear Kennedy et al. (2017) spin ephemeris (which is referenced to 2014.97) to create a spin-pulse O−C diagram, extending it as far back as possible before baseline curvature (due to $\dot{P}$) became apparent. We then fit the pulse timings within this window with a quadratic ephemeris, plotted an updated O−C diagram, and extrapolated it backwards in time until curvature reappeared in the O−C plot. By iteratively extrapolating a trial ephemeris towards older observations and increasing the polynomial order to flatten the O−C diagram, we eventually found an ephemeris that extends back to our earliest pulse timings in September of 2002:

$$T_{max}[BJD] = AE^4 + BE^3 + CE^2 + P_0E + T_0, \quad (1)$$

where $A = (9.61 \pm 0.44) \times 10^{-24}$, $B = (6.50 \pm 0.19) \times 10^{-18}$, $C = (1.86 \pm 0.18) \times 10^{-13}$, $P_0 = 0.0145177196 \pm 0.0000000016$ d, $T_0 = 2456977.105796 \pm 0.000025$ in the BJD_{TDB} standard, and E is the integer cycle count.

The spin period predicted by our ephemeris (*i.e.*, its first derivative) is consistent with unpublished, yearly measurements of the spin period by the Center for Backyard Astrophysics (CBA; see Patterson 2012), as well as the refined measurement of the *K2* spin period from Kennedy et al. (2017). We overlay these measurements of the spin period in Fig. 4. However, our ephemeris strongly disagrees with the Andronov et al. (2005) value of $P_{spin} = 1254.285(16)$ s at epoch 2004.6, which they derived by fitting a sinusoidal function to time-series photometry from 10 observing runs spread across a 26-day span. As discussed previously, attempts to measure FO Aqr's spin period by representing its light curve with trigonometric functions are susceptible to systematic errors and are less reliable than O−C analysis (Kennedy et al. 2017).

An important caveat with FO Aqr's pulse timings is that they show a great deal of jitter from cycle-to-cycle, such that the residuals from any spin ephemeris are frequently $\sim \pm 0.1$ in phase. Some of this is attributable to systematic contamination by the beat pulse (Osborne & Mukai 1989), the severity of which varies unpredictably

[2] The Bonnardeau (2016) photometry is available at https://konkoly.hu/pub/ibvs/6101/6181-t2.txt.

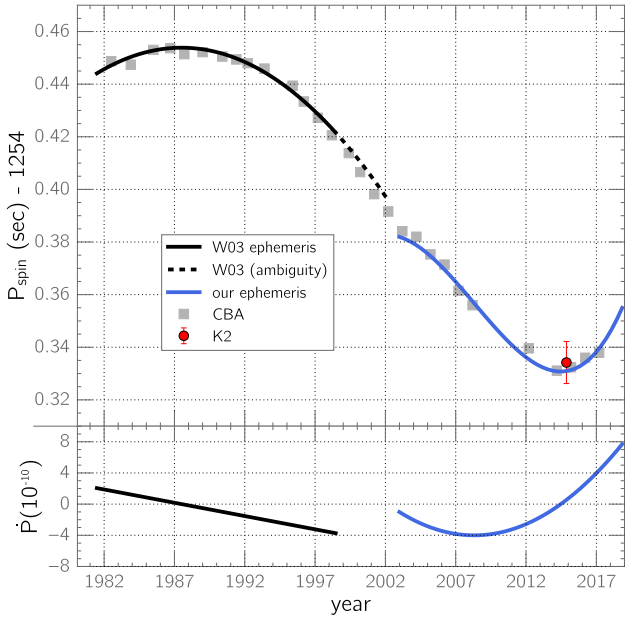

Figure 4. The spin period and $\dot{P}$ of FO Aqr since its discovery. The two solid lines are the first derivatives of different ephemerides: (1) ours, which extends from 2002–present, and (2) that of Williams (2003), which describes all pulse timings from 1981–2002 (albeit with a cycle-count ambiguity after 1998). A paucity of publicly available data from 1999-2003 prevents us from easily linking the two ephemerides, and the apparent discontinuity in $\dot{P}$ underscores the need to analyze all data together in order to produce a unified ephemeris. For reference, we also plot independent, yearly measurements of the spin period by the Center for Backyard Astrophysics as well as the *K2* spin period from Kennedy et al. (2017) to show that they agree with the first derivatives of the two ephemerides.

at different epochs (Patterson et al. 1998). There is also a dependence between pulse O−C and the brightness of the system (Kennedy et al. 2016). While a large number of pulse timings spread across many nights in a given season should cause these effects to average out, several of the observing seasons covered by our ephemeris contained only a few pulse-timing measurements that were extracted from several closely spaced time series. As a concrete example, the AAVSO dataset from 2002 contains 59 pulse timings obtained in a 7.1-day timespan. Fig. 7 in Kennedy et al. (2016) shows that on such a short timescale, all observed pulses could easily experience a uniform bias of ± ∼0.03 in phase, thereby mimicking the effect of an inaccurate spin period. While the resulting ephemeris might accurately predict the times of pulse maxima within the underlying dataset, it would not be measuring the actual rotation of the WD and would yield inaccurate predictions of the spin period and $\dot{P}$ near 2002.

Unfortunately, we cannot easily unify our ephemeris with that of Williams (2003), which has a cycle-count ambiguity after 1998 due to an observational gap between 1998–2002. In principle, it is feasible to use the yearly CBA spin periods to constrain and solve this problem. However, the optimal solution is to take the CBA photometry, extract times of pulse maxima, and include them in an O−C analysis of all available pulse timings from the literature. Such an analysis is beyond the scope of this paper.

4.2. *The correlation between low states and epochs of spin-down*

If we assume that the duration of spin-down and spin-up episodes are similar and extrapolate backwards, the low states in 1965, 1966, and 1974 would have occurred during the first ∼two-thirds of FO Aqr's previous spin-down epoch. We illustrate this in Fig. 5, which approximates the spin period with a sinusoid and extrapolates it back to the Harvard plate observations from Garnavich & Szkody (1988). Although a sinusoid is an imperfect approximation of the evolution of the spin period, it offers a more reliable means of extrapolation than the fourth-order polynomial in our spin ephemeris (Eq. 1).

Fig. 5 underscores that each of FO Aqr's observed low states has occurred while the WD has been in either an observed or a suspected state of spin-down; no low states have been detected during a spin-up episode despite excellent observational coverage. The extrapolated spin period suggests that the WD would have been spinning up during the most densely sampled portion of the Harvard Plate Archive light curve, and Garnavich & Szkody (1988) did not detect even a single low state during that interval. Likewise, FO Aqr has been well observed since its identification as an IP by Patterson & Steiner (1983), and for nearly that entire segment of its history, it was spinning up (Fig. 4). It was not until after the start of its current spin-down episode that it was observed in low-accretion states.

In Sec. 7.1, we discuss the implications of the WD's spin evolution.

5. OBSERVATIONS OF THE 2016, 2017, & 2018 LOW STATES

5.1. *Final recovery from the 2016 low state*

Paper I reported time-resolved photometry through 2016 September 27, but the recovery was still underway at that time. The extended baseline of our dataset reveals when and how that low state ended.

As shown in Fig. 6, the recovery entered a chaotic state in mid-September and remained that way until the end of October. During this time, the light curve showed

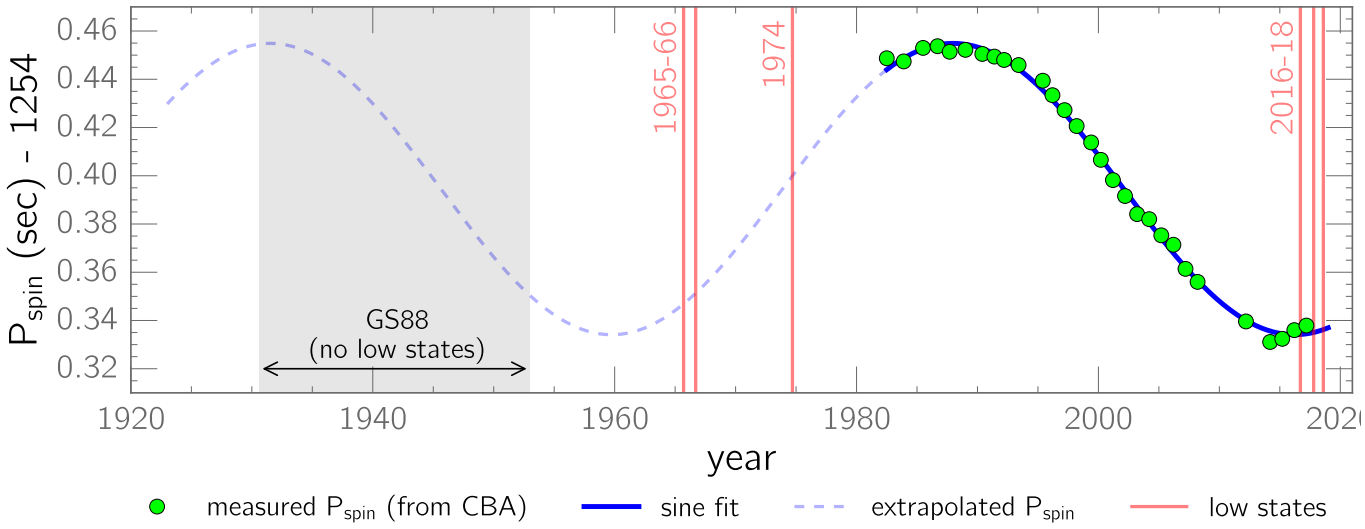

Figure 5. A sinusoidal extrapolation of the spin period, illustrating how the newly discovered low states from the 1960s and 1970s plausibly correlate with the WD's spin-down. The shaded gray region indicates the final 23 years of coverage from Garnavich & Szkody (1988), when the density of observations was sufficiently high to rule out the presence of low states. The yearly spin-period measurements were calculated by the Center for Backyard Astrophysics.

considerable scatter, suggestive of a series of flares and dips. This behavior is present in the data of the three most prolific data sources (the SLKT and AAVSO observers GKA and ATE) during this segment of the recovery.

The stall persisted until approximately 2016 Oct. 25, when there was a discontinuity in the light curve as the system abruptly surged to V$\sim$ 13.85. After this jump, the $\omega - \Omega$ and $2(\omega - \Omega)$ signals became very weak, with ω reemerging as the dominant short-period signal. The system did not continue to brighten thereafter, so the optical recovery was complete by the end of 2016 October.

The eclipse depth gradually increased during the recovery. By phasing all data on the orbital period, we isolated the orbital modulation from the other variability in the light curve (Fig. 7). In July 2016, the eclipse depth was 0.16$\pm$0.01 mag, and between August 1 - Sept. 30, it was 0.19$\pm$0.01 mag. Since we lack intensive observations of the deepest part of the low state, the current dataset does not constrain the behavior of the eclipse during the deepest part of the low state.

The end of the 2016 low state provides a useful context for the *XMM-Newton* observations of FO Aqr reported by Kennedy et al. (2017). Obtained on 2016 November 13-14, those data captured the system just over two weeks after the end of the optical low state. Although the X-ray luminosity had not returned to its 2001 level in those observations, the X-ray power spectrum was consistent with disk-fed accretion (Kennedy et al. 2017).

5.2. *The Short-Lived 2016-17 High State*

5.2.1. *Optical photometry*

Following the completion of its recovery, FO Aqr entered into a high state at the beginning of 2016 November. ASAS-SN photometry shows that between 2016 November 1 and 2017 August 1, its average magnitude was $V = 13.72\pm0.02$, compared to $V = 13.565\pm0.008$ in three years of ASAS-SN observations prior to the 2016 low state. Each of these uncertainties is the standard error of the mean magnitude. This 0.15-mag differential establishes that FO Aqr never fully recovered to its pre-low-state optical luminosity.

Although the 2016-17 high state was somewhat fainter than usual, it still showed the hallmarks of FO Aqr's original high state. The dominant periodicity was at ω, and the pulsation amplitude peaked at 0.4-0.5 mag. The power spectra obtained during this period do not show any significant power at $\omega - \Omega$, its harmonics, or other sidebands of ω, consistent with a return to disk-fed accretion.

The phase-averaged orbital profile of the 2016-17 high state differs from that observed during the pre-2016 high state, as shown in Fig. 8. We use the *K2* dataset, which spanned from 2014 Nov. 15 - 2015 Jan. 23, to measure the waveform prior to the low state. A close examination of the *K2* waveform shows that it varied in response to small ($\sim$0.15 mag) changes in the overall brightness during the *K2* observations (Fig. 8, top panel).

5.2.2. *X-ray observations*

The 2017 *XMM-Newton* observations bolster our conclusion that the system never fully recovered to its pre-2016 state. We simultaneously fit the EPIC-pn,

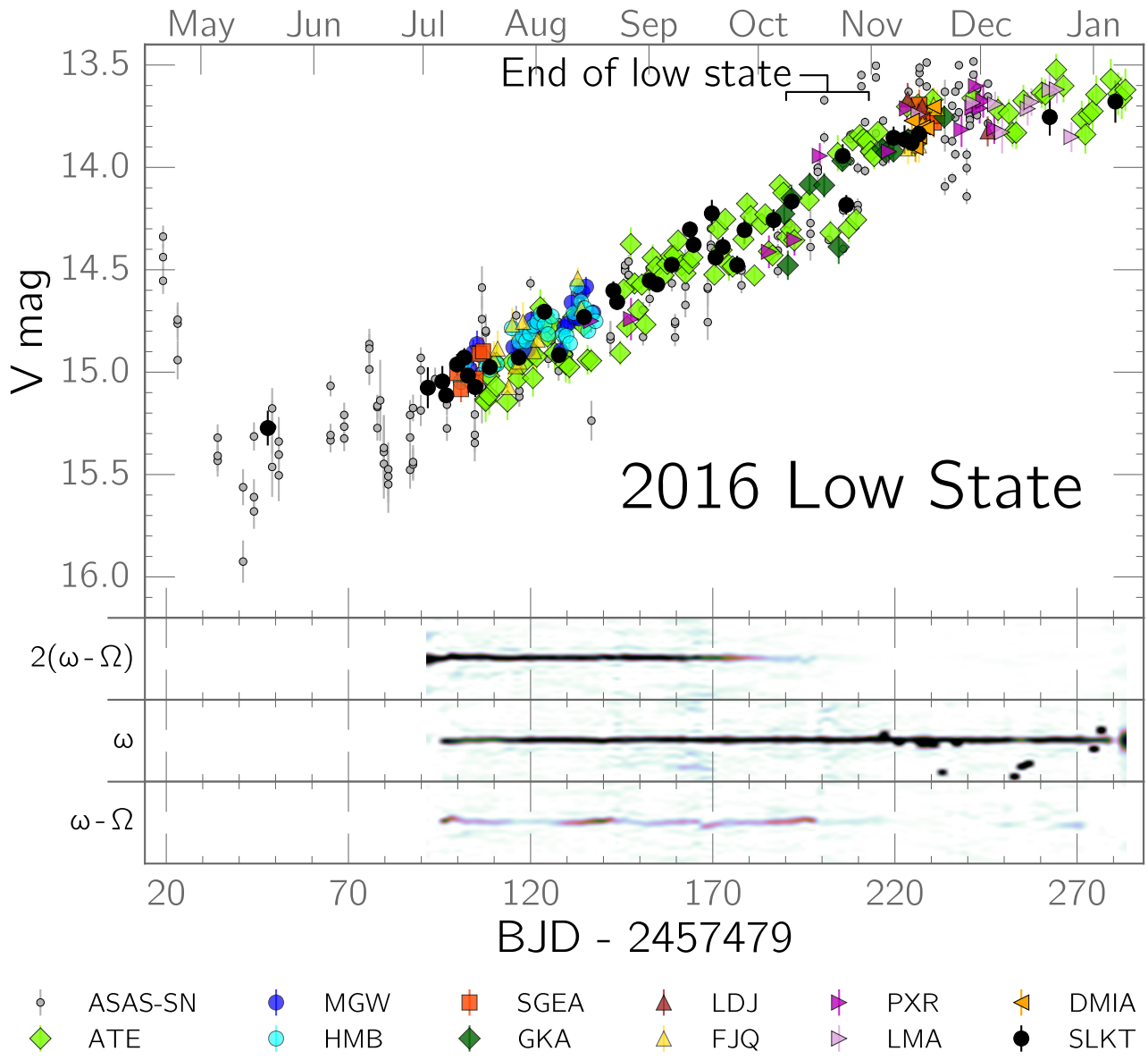

Figure 6. Light curve of the 2016 low state, with trailed power spectra of the three major short-term periodicities. Each point is the average magnitude of a time series, and each errorbar is a 1σ estimate of the overall brightness, based on the duration of each individual time series and Monte Carlo simulations as described in the text. The different symbols correspond to various observers. The beginning of each month is indicated along the top of the figure. The power at both $\omega - \Omega$ and $2(\omega - \Omega)$ drops precipitously at about the same time that the light curve jumps ~0.5 mag to the high state.

MOS1, and MOS2 spectra with the same model used by Kennedy et al. (2017) to analyze the 2016 observation: two separate MEKAL components, a GAUSSIAN to model the 6.4 keV Fe line, an interstellar absorber, and two circumstellar absorbers, each with its own covering fraction. The 2017 spectrum is shown in Fig. 9, along with the 2001 and 2016 spectra for comparison. The best-fit parameters of the 2017 spectrum, which are listed in Table 1, are statistically indistinguishable from those describing the *XMM-Newton* spectrum of the 2016 high state (Table 2 in Kennedy et al. 2017). The similarity between the 2016 and 2017 X-ray spectra suggests that the soft X-ray excess noted in Kennedy et al. (2017) might be a lasting consequence of the low states.

The X-ray light curve and power spectrum (Fig. 10) show that the soft X-rays are strongly pulsed, with the count rate typically dropping to zero between spin pulses. Kennedy et al. (2017) noted similar behavior, but the pulses in the soft X-ray light curve in the 2016 high state were far more sporadic than in the 2017 light curve. Indeed, during the three partial orbits covered in the 2017 light curve, the soft pulses were visible through-

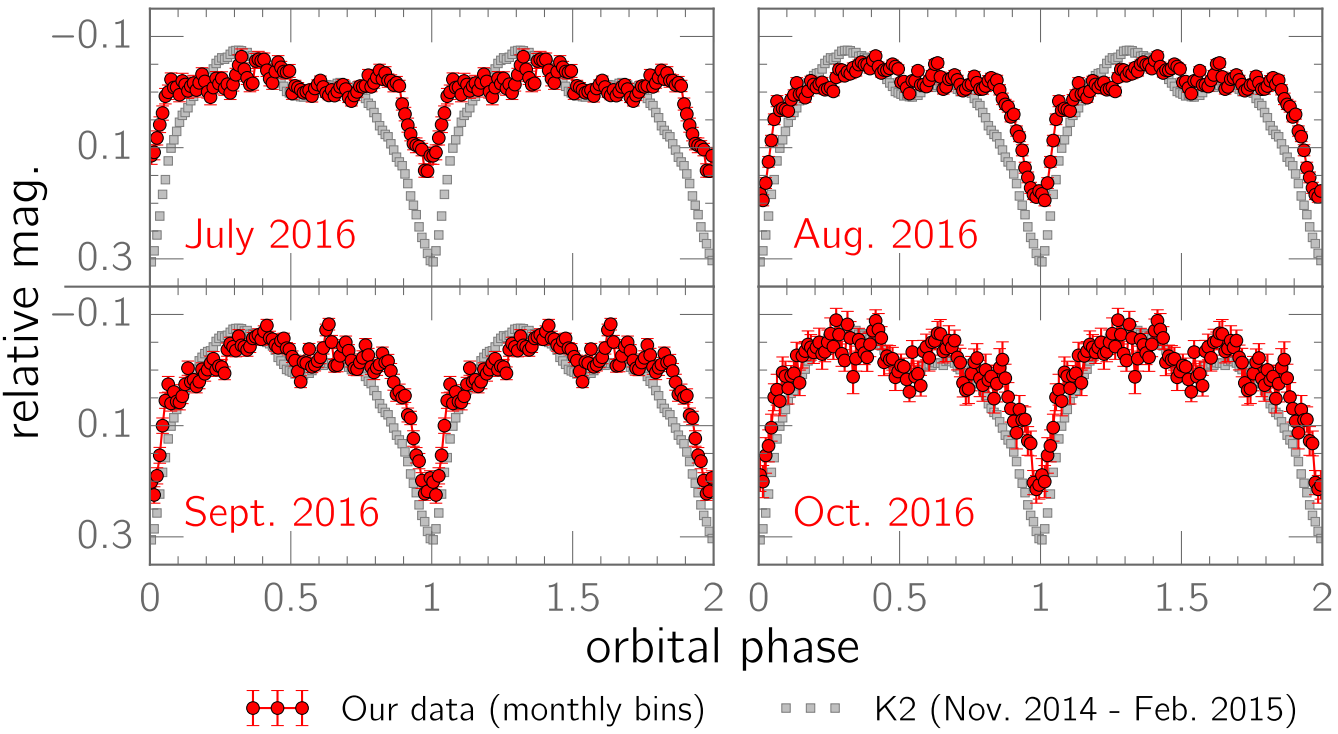

Figure 7. Phase-averaged profiles of the eclipse during the 2016 low state. The *K2* orbital waveform is plotted for reference. The eclipse depth was lowest in July 2016, when the system was faintest.

Table 1. Best-fit X-ray spectral parameters (2017)

Component	Parameter	Value
WABS	nH	$0.13^{+0.05}_{-0.03} \times 10^{22}$
PCFABS$_1$	nH	$15.4^{+1.7}_{-1.4} \times 10^{22}$
	cvf	$0.72^{+0.02}_{-0.04}$
PCFABS$_2$	nH	$3.4^{+0.4}_{-0.3} \times 10^{22}$
	cvf	$0.89^{+0.01}_{-0.01}$
MEKAL$_1$	kT	$36.6^{+10.8}_{-5.3}$ keV
	norm	$0.03034^{+0.00092}_{-0.00083}$
MEKAL$_2$	kT	$0.118^{+0.014}_{-0.011}$ keV
	norm	$0.018^{+0.013}_{-0.007}$
GAUSSIAN	center	$6.485^{+0.021}_{-0.024}$ keV
	σ	$0.179^{+0.040}_{-0.019}$
	norm	$1.29^{+0.21}_{-0.12} \times 10^{-4}$

NOTE—The full model was WABS * PCFABS$_1$ * PCFABS$_2$ * (MEKAL$_1$ + MEKAL$_2$ + GAUSSIAN). In addition to the free parameters listed above, each MEKAL component had four fixed parameters: nH = 1 cm^{-3}, abundance = 0.5, redshift = 0.0, and switch = 1.

out the first two orbits except during orbital phases 0.8-1.0, when there was an energy-dependent drop in the pulse amplitude. This is consistent with photoelectric absorption of the soft X-rays caused by vertical disk structure, possibly related to the stream-disk collision. Since the optical eclipse is centered on orbital phase 0.0, this effect cannot be attributed to an eclipse by the secondary. A more likely candidate is a large, dense bulge in the disk. de Martino et al. (1994) proposed such a structure in order to explain an optical $\omega - \Omega$ signal during a time of disk-fed accretion.

It is also remarkable that the soft pulses became dramatically weaker and more intermittent during the third orbit, establishing that the absorbing structure can vary on equally fast timescales.

5.3. *The 2017 Low State*

Unlike the 2016 low state, which was detected only after FO Aqr had faded to its minimum brightness, the 2017 event was noticed almost immediately (Littlefield et al. 2017), and there is high-quality time-series photometry of the system before, during, and after the transition into the low state. Although the coverage of the beginning was excellent, the low state was still underway when FO Aqr reached solar conjunction, so the end of the 2017 low state was unobserved. Fig. 11 shows the light curve and trailed power spectrum of the 2017 event, while Fig. 12 presents monthly phase-averaged eclipse profiles.

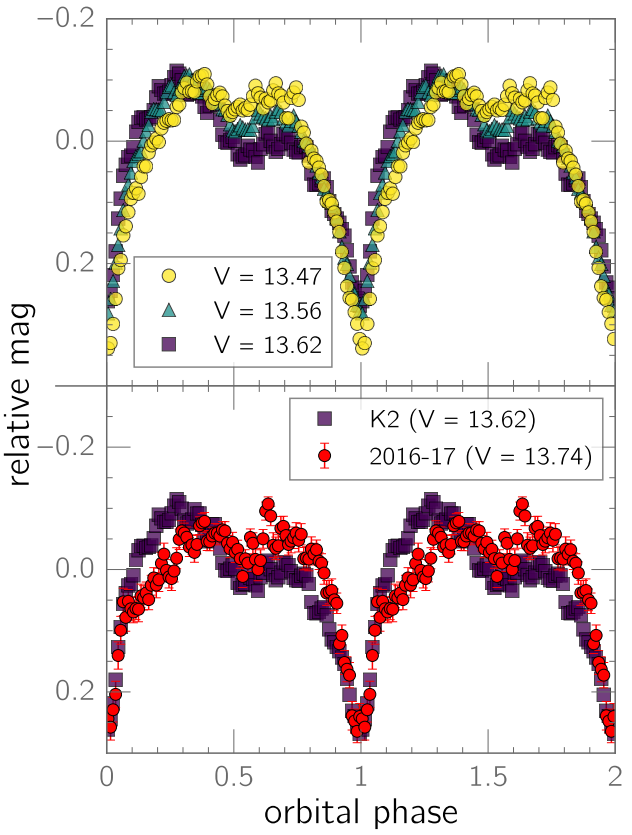

Figure 8. Top: Phase-averaged orbital profiles from the high state observed by *Kepler* in its *K2* mission. The data were split into bins based on their mean brightness. The pre-eclipse light curve became brighter as the system brightened. **Bottom:** The orbital profile of the 2016-17 high state compared against the faintest bin from *K2*. In both panels, the average V magnitude for each dataset was determined from contemporaneous ASAS-SN photometry.

Whereas the 2016 low state was characterized by a steady, gradual recovery throughout the observations, the 2017 low state featured an irregular, slow fade followed by a comparatively rapid rebrightening as solar conjunction approached. The most remarkable feature in the light curve is a conspicuous, ∼0.4-mag fade at the start of the low state whose abruptness provided a stark contrast to the laconic pace of the fading during the rest of the 2017 event.

Because the trailed power spectra in Fig. 11 utilize a two-week sliding window, they show overall trends in the power spectrum and do not describe any individual time series. Consequently, inspecting the power spectra of individual time series often reveals transient changes that are not apparent in the trailed spectra. For example, the light curve in Fig. 11 identifies two particular time series that appear to be part of the same flaring event. Additionally, the time series immediately before the flare was the first to be obtained after the drop into the low state, and it was also the first to show measurable power at $2(\omega - \Omega)$.

5.4. *The 2018 Low State*

ASAS-SN observations show that FO Aqr was in a high state as it emerged from solar conjunction in April 2018. In mid-May, it faded by ∼0.4 mag (Littlefield et al. 2018). During this interval, ASAS-SN observed the system sporadically, but the sparse sampling precludes meaningful power spectral analysis. Time-series photometry of this low state began in earnest in late May, picked up in early-to-mid June, and became prolific at the start of August after an AAVSO campaign was launched. Fig. 13 presents the light curve of the 2018 low state, and it is immediately obvious that the 2018 event was briefer and shallower than its two predecessors, lasting only $\lesssim$3 months and dropping just ∼0.5 mag relative to its brightness before the low state.

The start of intensive AAVSO coverage in August fortuitously coincided with the system's recovery to a bright state, and the light curve showed a series of flares and dips, each lasting a few days, as the system vacillated between the low and high states. During these flares, individual time series showed an intermittent spin pulse that dominated the light curve when present.

Phase-averaged orbital light curves of the 2018 low state (Fig. 14) confirm that, as with the 2016 and 2017 low states, there was an eclipse.

5.5. *The late 2018 high state*

After the series of flares in mid-August, FO Aqr completed its recovery and remained at $V \sim 13.9$ for approximately one month. During this time, ω was consistently the only significant short-term periodicity. In mid-September, the system brightened by another ∼0.2 mag but did not show any contemporaneous changes in its behavior.

One notable feature of the 2018 high state is that the amplitude of the spin pulse was lower by $\sim$ 0.05 mag in comparison to the 2016-17 high state. In Fig. 15, we plot phase-averaged profiles of the spin pulse based on our spin ephemeris. Despite the decreased pulse amplitude, the morphology of the pulse remained sinusoidal in each of the observed high states. Conversely, the spin profiles obtained during the 2016 and 2017 low states experienced a modest phase shift towards later phases ($\Delta\phi_{spin} \sim 0.05$) and were asymmetric, with the rise to maximum being slower than the decline from maximum.

6. STROBOSCOPIC ORBITAL LIGHT CURVES

The simultaneous presence of multiple short-term periodicities complicates efforts to study any one of those

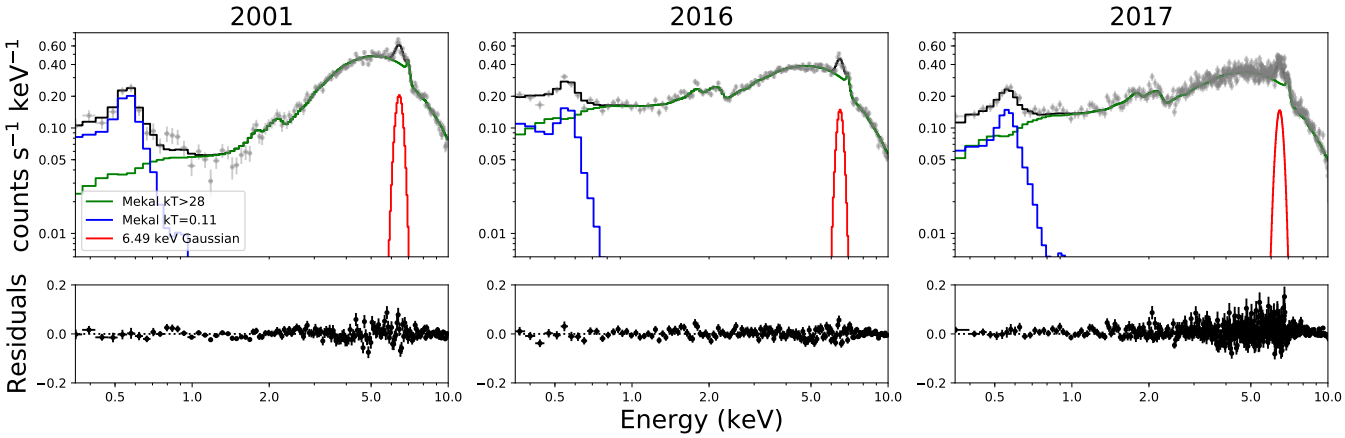

Figure 9. The high-state X-ray spectrum of FO Aqr at three different epochs, obtained with XMM Newton's EPIC-pn instrument. The spectra in the left and central panels were originally reported in Evans et al. (2004) and Kennedy et al. (2017), respectively. The newly reported spectrum is in the right panel.

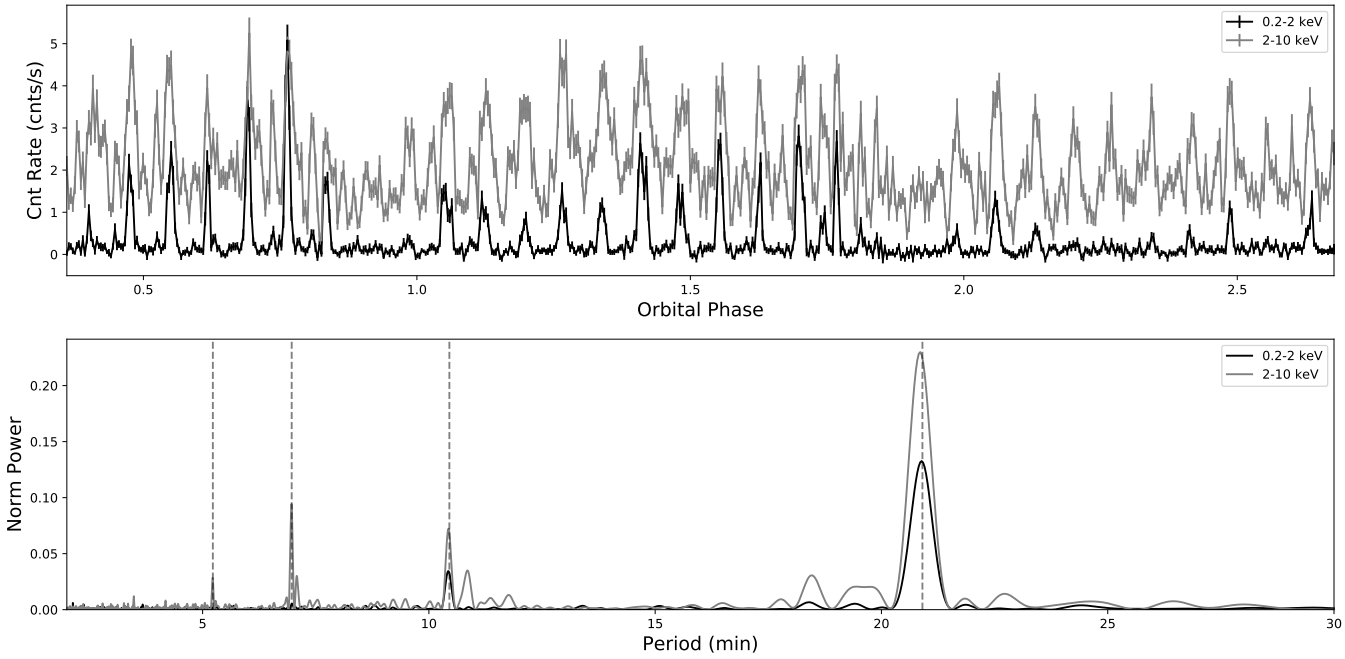

Figure 10. The 2017 XMM-Newton light curve of FO Aqr and its Lomb-Scargle power spectrum. The pulsed hard X-ray flux is significantly attenuated shortly before the predicted time of mid-eclipse. Unlike the long-term high state, soft X-ray pulses were routinely observed, albeit with an orbital-phase dependency. The strongest signal in both the hard and soft X-ray light curves is the 20.9-minute spin period. The spin signal and its first 3 harmonics are all marked with dashed vertical lines.

periods independently of the others. In their spectroscopic examination of FO Aqr, Marsh & Duck (1996) addressed this issue by analyzing the spectra as a function of the spin-orbit beat phase. The beat phase describes the relative orientation of the WD with respect to the secondary, so if the data are split into small bins according to their beat phase, each bin will describe the system at one particular accretion geometry. Marsh & Duck (1996) compared this technique to using a stroboscope to "freeze" the rotation of a fast-spinning object, and it allows us to examine how the rotation of the WD interacts with the orbital light curve.

We show stroboscopic light curves of both the spin and beat modulations in Fig. 16. We define beat phase 0.0 as the accretion geometry during which the upper mag-

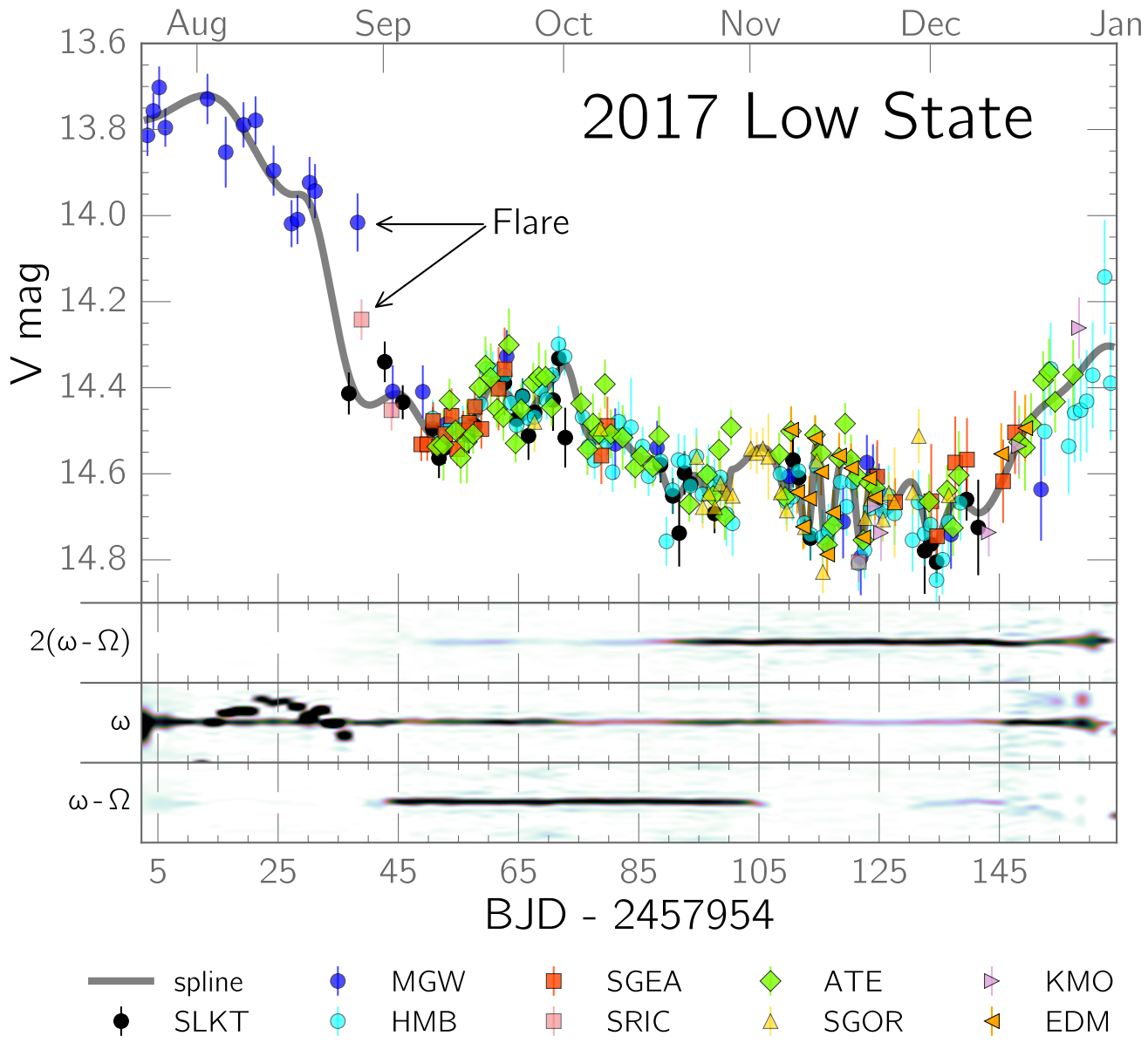

Figure 11. As with Fig. 6, but for the 2017 low state. There was a gradual fade in early-to-mid August, followed by an abrupt drop into the low state. The magnitude at which this break in the light curve occurred, V∼14, is very close to the magnitude at which Hameury & Lasota (2017) expect the accretion disk to disappear.

netic pole tilts away from the companion.[3] The complex structure of these stroboscopic light curves yields insight into the interplay between FO Aqr's spin, beat, and orbital periods. For example, in the high state, the eclipse depth varies dramatically as a function of spin phase, with maximum depth occurring at $\phi_{spin} \sim 0.5$, the minimum of the spin pulse. This is fully consistent with the eclipse depth being diluted by light from the spin pulse, in agreement with the widely accepted viewing geometry in which the upper accretion curtain produces the spin pulse and is never eclipsed by the companion. Likewise, the stroboscopic, low-state beat light curves show two peaks near $\phi_{beat} \sim 0.3$ and $\phi_{beat} \sim 0.8$, as might be expected from a magnetic dipole accreting from a stationary source in the binary rest frame.

The stroboscopic light curves in Fig. 16 also offer an explanation for why the high-state *K2* orbital waveform in Figs. 7, 12, and 14 is double-humped: the amplitude of the spin pulse changes across the orbit during the high state. Although phase-averaging the light curve to the orbit will smear out individual pulses, this tech-

[3] We presume that this occurs when the spin pulse occurs at an orbital phase of 0.0.

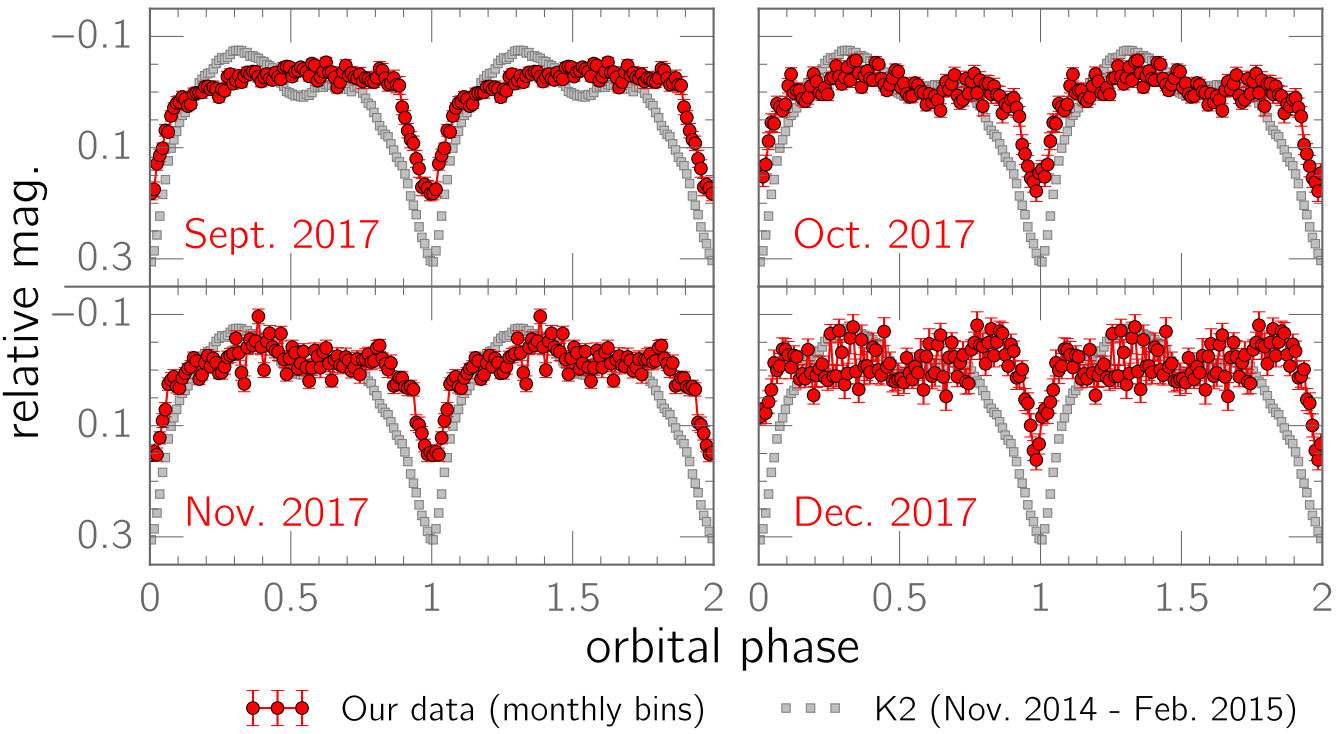

Figure 12. Phase-averaged profiles of the eclipse during the low state in 2017. The changes in eclipse depth are less pronounced than in the 2016 event, which was significantly deeper.

nique does not compensate for the increased contribution from the spin pulses near orbital phases ∼0.3 and ∼0.7, creating the appearance of an orbital brightening. If the system could be observed at the minimum of the spin pulse across the entire orbit, the out-of-eclipse light curve would not show the double-humped waveform (Fig. 16).

7. DISCUSSION

7.1. *Spin period*

A major theoretical prediction about IPs is that angular momentum flows within the system should cause the WD's spin period to evolve to an equilibrium value, usually expressed as a fraction of the orbital period. This equilibrium is achieved when the spin-up torque from accretion equals the spin-down torque caused by the drag of the WD's magnetic field on the accretion flow, and the resulting P_{spin}/P_{orb} ratio depends on whether the accretion is usually disk-fed or stream-fed (e.g., King & Lasota 1991; Warner & Wickramasinghe 1991). Expressed in terms of the circularization radius (R_{circ}), the corotation radius (R_{co}), and the distance from the WD to the $L1$ point (R_b), there are two types of equilibria in a diskless geometry: $R_{co} \sim R_{circ}$, which gives $P_{spin}/P_{orb} \sim 0.07$, and $R_{co} \sim R_b$, which yields $0.1 \lesssim P_{spin}/P_{orb} \lesssim 0.68$, depending on the mass ratio (King & Wynn 1999). In a disk-fed geometry, the equilibrium condition is $R_{co} \sim R_{in}$, where R_{in} is the inner radius of the disk (King & Lasota 1991). The resulting P_{spin}/P_{orb} can take a wide range of values but will be smaller than the diskless $R_{co} \sim R_{circ}$ equilibrium (Warner & Wickramasinghe 1991).

The spin period of an IP in equilibrium can exhibit small oscillations with respect to its equilibrium value if, for example, $\dot{M}$ varies coherently on timescales of years (Warner 1990). Thus, equilibrium rotation should cause $\dot{P}$ to undergo sign reversals on timescales of years as the WD alternates between episodes of spin-up and spin-down (Patterson 1994). For IPs that are in spin equilibrium, the WD's magnetic moment μ can inferred from knowledge of P_{spin} and P_{orb} (Norton et al. 2004, their Fig. 2).

The evolution of $\dot{P}$ in FO Aqr—featuring two sign reversals only ∼25 years apart—offers compelling evidence that the system is in spin equilibrium. As shown in Fig. 4, the spin period has shown a quasi-sinusoidal variation since the early 1980s, with a maximum period near 1988 and a minimum period in 2014. The short timescale for the transition from spin-down to spin-up to spin-down is strong evidence that FO Aqr's spin period is very close to its equilibrium value. The observed spin-period oscillations are probably related to long-term modulations in the mass-transfer rate, an inference bolstered by the fact that the 2016, 2017, and 2018 low

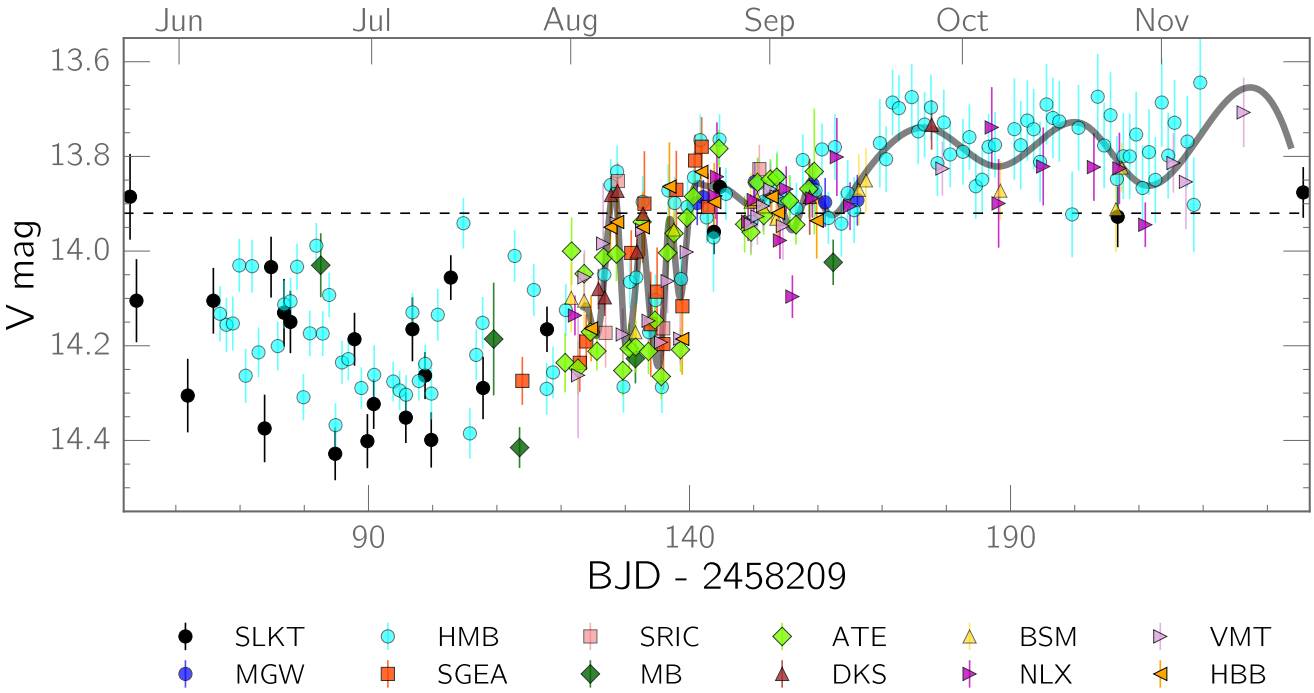

Figure 13. As with Figs. 6 and 11, but for the 2018 low state. The horizontal dashed line represents FO Aqr's brightness in pre-low state ASAS-SN photometry obtained in 2018. The spline fit is meant to guide the eye and models only the most densely sampled part of the light curve. We omit the trailed power spectrum because of the comparatively sporadic coverage of the 2018 low state and because the sliding window size is too wide to resolve the rapid changes observed during the flaring observed in early August. In these three, ∼0.3-mag flares, FO Aqr briefly reattained its pre-low-state brightness. The low state ended in mid-August, and approximately one month later, FO Aqr brightned by an additional 0.2 mag.

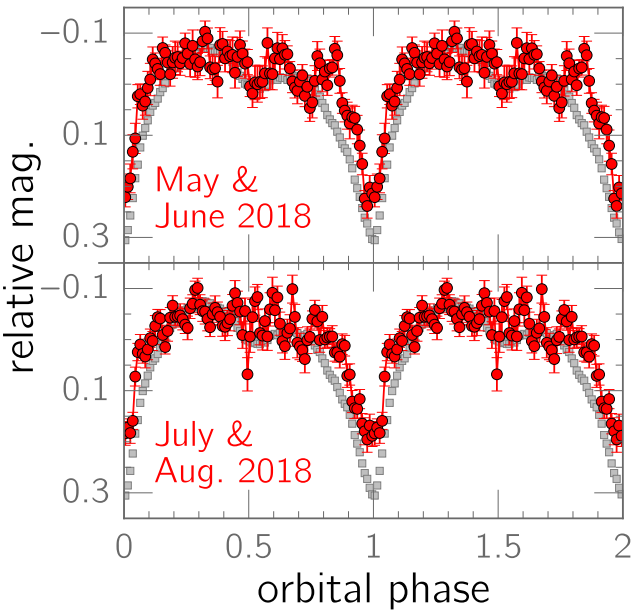

Figure 14. Phase-averaged orbital profiles of the 2018 low state. The data used in the lower panel were all obtained before the start of the flaring episodes visible in Fig. 13. As with Figs. 7 and 12, the gray points are the average *K2* profile.

states occurred almost immediately after the WD began spinning down. If we were to interpret the ∼quarter-century duration of the spin-up episode as half of the $\dot{P}$ cycle, the implied half-century quasi-periodicity would be reminiscent of the expected timescale for magnetic-activity cycles in CV secondary stars (Warner 1988), which Warner (1990) argued were a likely culprit for decade-long variations in $\dot{P}$ in IPs.

Warner (1990) pointed out that changes in $\dot{P}$ are expected to be accompanied by changes in the system's bolometric luminosity. It is unclear whether these changes would be readily detectable in the optical, where a gradual brightening or dimming by several tenths of a magnitude could easily be obfuscated by a combination of the system's short-period variability and the heterogeneity of the sources of the existing data. Although Warner (1990) noted an apparent ∼0.3-mag variation in the 1923-1953 light curve from the Harvard Plate Collection (Fig. 1 in Garnavich & Szkody 1988), there is no simultaneous information on $\dot{P}$ against which to compare that light curve.

7.2. *Spin-down power*

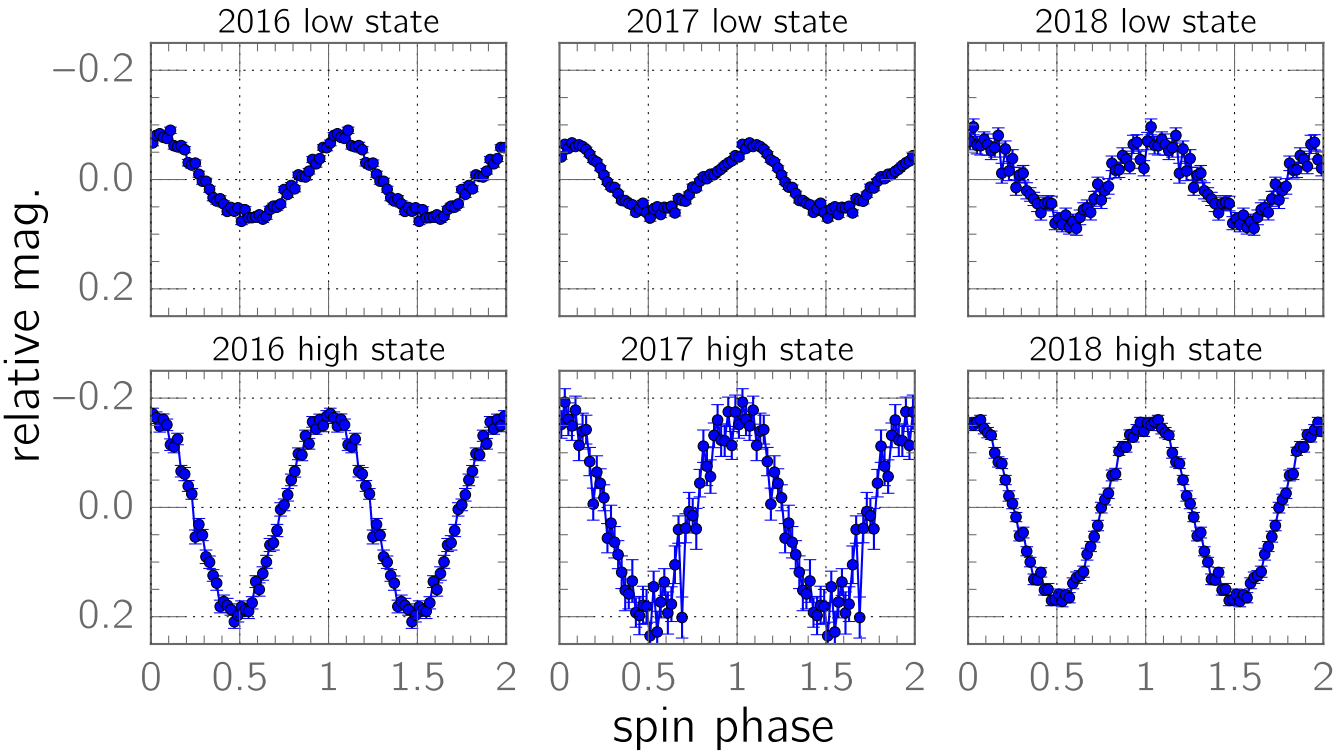

Figure 15. Phase-averaged spin profiles of each low and high state. In the 2016 and 2017 low states, the amplitude of the spin pulse was much lower, the pulse maximum was somewhat sawtooth-shaped, and the maximum occurred slightly after phase 0.0. Conversely, in each high state, the spin pulse was nearly sinusoidal and centered on phase 0.0. However, its peak-to-peak amplitude of 0.4 mag in 2016 and 2017 decreased to 0.3 mag in 2018.

The power generated by the spin-down of a WD is given by Marsh et al. (2016) as

$$P_{\dot{\nu}} = -4\pi^2 I \nu \dot{\nu}, \tag{2}$$

where I is the WD's moment of inertia, ν is the rotational frequency, and $\dot{\nu}$ is the rotational-frequency derivative. For an assumed WD mass of 0.8 $M_\odot$ and radius of 0.01 $R_\odot$, $I = 0.25MR^2 = 2 \times 10^{43}$ kg m^2, and from this, we calculate that $P_{\dot{\nu}} \approx 2 \times 10^{26}$ J/s $\sim 0.5\ L_\odot$ for a representative period derivative of $\dot{P} = 4 \times 10^{-10}$ from Fig. 4.

We do not know where this energy is being deposited, but if it were driving a wind from the system, the resulting decrease in the accretion rate might help to explain why FO Aqr's low states correlate with the WD's spin-down, particularly in light of calculations by Hameury & Lasota (2017) that FO Aqr's high-state mass-transfer rate is only several times above the threshold at which the accretion disk would dissipate (see Sec. 7.4). Any such wind would likely be detectable as a line-absorption component in ultraviolet spectroscopy.

7.3. *Mode of accretion*

Together, the 2016, 2017, and 2018 datasets showcase the gradual evolution of FO Aqr's power spectrum. To underscore this point, Fig. 17 plots the power spectrum across different intervals across the three years. Observations during the deepest portion of the 2016 low state showed a very strong signal at $2(\omega - \Omega)$ that gradually faded away as the system rebrightened, eventually disappearing altogether when FO Aqr returned to a high state in late 2016 October. During this high state, ω was the only major, short-period signal in the light curve, but when the system fell into another low state in late 2017 August, $\omega - \Omega$ became prominent in the power spectrum, rivaling ω. As the low state progressed, power gradually shifted from $\omega - \Omega$ to $2(\omega - \Omega)$. The 2018 observations continued this pattern; there was a significant signal at $\omega - \Omega$ in the low state, but it vanished during the ensuing high state, replaced by ω.

These changes in the power spectrum are fundamentally linked to the processes by which the accretion flow couples to the WD's magnetic field. Ferrario & Wickramasinghe (1999) simulated the differences in optical power spectra of disk-fed and stream-fed CVs, finding that power at $\omega - \Omega$ and $2(\omega - \Omega)$ indicates that a fraction of accretion is stream-fed. Although an amplitude modulation of ω at the orbital frequency can transfer power from ω to $\omega - \Omega$, this mechanism would also produce a comparable signal at the upper orbital sideband,

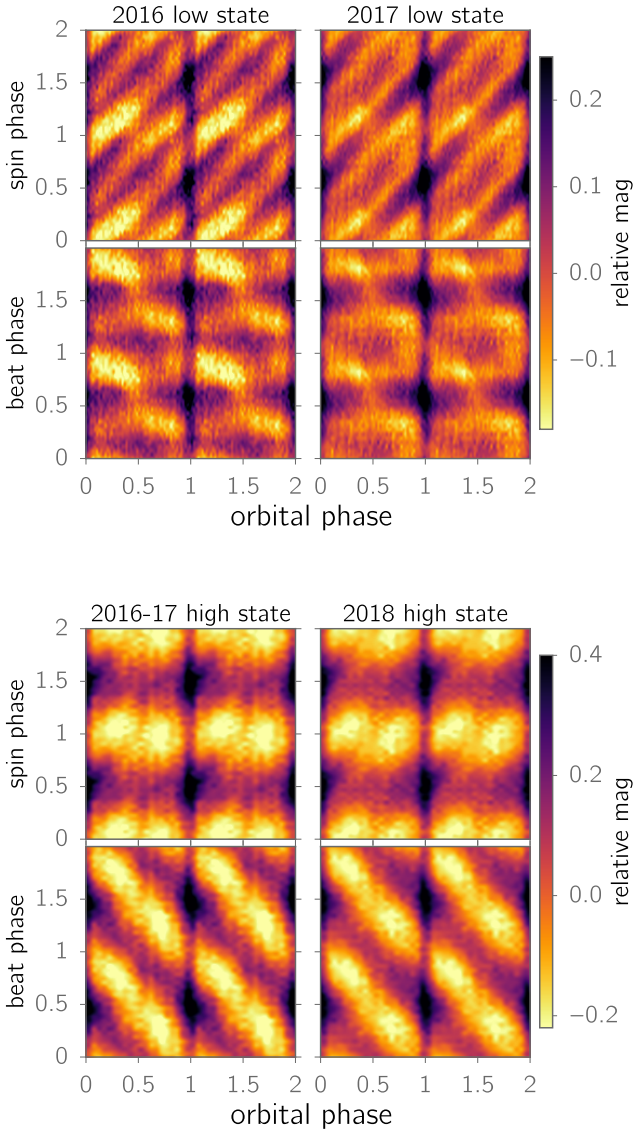

Figure 16. Two-dimensional, stroboscopic light curves of each low state (top row) and high state (bottom row) in our dataset; note that the dynamic range represented by the colormap is different for the two rows. A horizontal slice through one of the panels gives the orbital light curve at a fixed spin or beat phase, while a vertical slice yields the spin or beat light curve at a fixed orbital phase. During the low states, the eclipses were deepest when the beat phase was ∼0.6.

$\omega + \Omega$ (Warner 1986); similarly, an amplitude modulation of 2ω at 2Ω would shift power to both $2(\omega - \Omega)$ and $2(\omega + \Omega)$. However, there is little power at the upper sidebands, indicating that neither $\omega - \Omega$ and $2(\omega - \Omega)$ can be entirely attributed to an amplitude modulation of the spin pulse and that the beat signals are instead intrinsic.

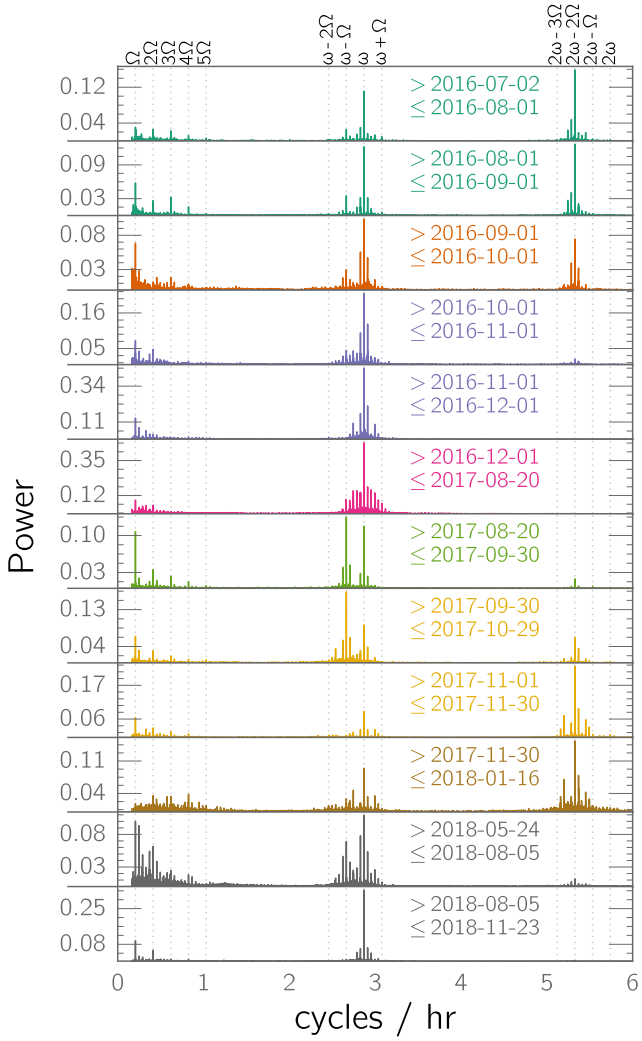

Figure 17. Lomb-Scargle power spectra of FO Aqr during different time bins.

Following this line of reasoning, Paper I determined that a significant fraction of the accretion in the 2016 low state was stream-fed, a conclusion substantiated by subsequent X-ray observations (Kennedy et al. 2017). The 2017 and 2018 low states showed a similar transfer of power from ω to $\omega - \Omega$ and $2(\omega - \Omega)$, so we conclude that in all three low states, there was significant interaction between the accretion stream and the magnetosphere. Although Murray et al. (1999) proposed that tidally-induced spiral structure in the inner disk could produce optical modulations at $2(\omega - \Omega)$ in IPs, their mechanism presupposes the presence of a viscous accretion disk, a scenario that the calculations of Hameury & Lasota (2017) rule out (Sec. 7.4). Moreover, it would be difficult to explain why the spiral structure would be present in the faint state but not in the high state, when the disk viscosity would be highest.

The nature of the signal at ω is more difficult to interpret. It cannot simply be an amplitude modulation of $\omega - \Omega$ at the orbital frequency since this would cause $\omega - 2\Omega$ to be of comparable strength to ω, which is contrary to our observations. Instead, Paper I interpreted the presence of ω during the low state as evidence that the WD accreted from an accretion disk—or perhaps more accurately in hindsight, from an azimuthally symmetric, circumstellar structure that is not necessarily Keplerian. This caveat is a consequence of the compelling theoretical argument by Hameury & Lasota (2017) that a Keplerian accretion disk could not have survived FO Aqr's 2016 low state, and as we discuss in detail in Sec. 7.4, it is likely that the circumstellar structure was a non-Keplerian ring of diamagnetic blobs.

In each transition between the high state and the low state, the power spectrum underwent an abrupt, fundamental transition at the same time as the light curve. When $\omega - \Omega$ disappeared from the power spectrum in 2016, the light curve abruptly jumped by ~ 0.4 mag, marking the end of the low state; likewise, when $\omega - \Omega$ reappeared in 2017, the light curve immediately dropped $\sim$0.4 mag into a low state. In both instances, there was a discontinuity in the light curve associated with a concomitant change in the mode of accretion. This suggests that the mode of accretion and the luminosity state of the system are intertwined, the implications of which we explore in Sec. 7.4.

7.4. *The likely dissipation of the disk*

Hameury & Lasota (2017) predicted that the accretion disk dissipated during the 2016 low state, a scenario that could explain the simultaneous discontinuities in the optical light curve and power spectrum. Motivated by the lack of dwarf-nova outbursts during FO Aqr's 2016 low state, they modeled the thermal state of the accretion disk during the low state and considered three possibilities: that the disk is always in a cold state, that it is always in a hot state, and that it is in a hot state but dissipates during the low state, causing the accretion stream to directly impact the magnetosphere. They showed that the first option was implausible and that although the second option was a remote possibility, it would require (1) the high-state $\dot{M}$ to exceed the expected evolutionary value by two orders of magnitude and (2) FO Aqr's distance to exceed 1 kpc, highly inconsistent with the subsequently determined Gaia DR2 distance of 518^{+14}_{-13} pc. Instead, they argued that the disk radius gradually shrank towards the circularization radius until it disappeared, an event predicted to occur when the system's optical magnitude dropped to $V \sim 14$ (based on the parameters assumed in their Fig. 5).

It is essential to note that the ubiquitous term "diskless accretion" is a misnomer; both observation (e.g., V2400 Oph: Hellier & Beardmore 2002) and theory (King & Wynn 1999) show that nominally diskless accretion in an IP can produce a ring-like structure around the WD. Unlike a bona-fide accretion disk, however, this ring consists of diamagnetic blobs whose motion is non-Keplerian and heavily influenced by a drag force exerted by the WD's magnetic field (King & Wynn 1999). As a result, a "diskless" accretion geometry can exhibit many of the hallmarks of disk-fed accretion, such as eclipses of a disk-like structure and a spin pulse. Thus, the presence of the disk in monthly, phase-averaged eclipse profiles of the low states (Figs. 7, 12, 14) is not prima facie evidence of an accretion disk, as the eclipses tell us nothing about the velocity field of the eclipsed matter. Because of the counterintuitive nature of the term "diskless accretion," we will hereafter refer to it as blob-fed accretion.

Returning to the data, the disk-dissipation model offers a coherent explanation for many of the key photometric properties of FO Aqr's three low states. One of our major findings is that in each well-observed transition into or out of a low state, there was a discontinuity in the light curve near $V \sim 14.0$, accompanied by a simultaneous change in the power spectrum (ω-dominated for $V \lesssim 14.0$ and $\omega - \Omega$-dominated for $V \gtrsim 14.0$). Hameury & Lasota (2017) predicted that at $V \sim 14$, the corresponding $\dot{M}$ would be low enough to cause the magnetospheric radius to exceed the circularization radius, disrupting the disk. A magnetosphere large enough to reach the circularization radius is necessarily large enough to intersect the ballistic trajectory of the accretion stream, and a ring of blobs would likely be too tenuous to stop the stream before its collision with the magnetosphere. Consequently, a blob-fed geometry would naturally account for the abrupt switch from a ω-dominated optical power spectrum to one with greatly elevated power at $\omega - \Omega$ and $2(\omega - \Omega)$. Moreover, it is natural to expect that when the accretion flow transitions from a viscous, disk-fed regime to being blob-fed, there could be a sudden drop in the optical luminosity, similar to the one that we observed. Conversely, the stream-overflow model (which presumes the presence of an accretion disk) does not offer a clear reason why there should be a break in the overall light curve or why it should coincide with a major and abrupt change in the power spectrum.

In addition, an accretion disk would respond to the diminished $\dot{M}$ on its viscous timescale ($\sim$10 d per Fig. 3 in Hameury & Lasota 2017), so we would expect the dis-

sipation of the disk to be preceded by a gradual fade on a similar timescale. We observed exactly this behavior prior to the start of the 2017 low state, as FO Aqr faded by 0.2 mag over the course of ∼15 d immediately before the discontinuity in its light curve (Fig. 11). There was no change in the power spectrum during this interval, implying that disk-fed accretion continued unabated.

Following the end of the 2018 low state, the system showed similar behavior, except in reverse; the light curve leveled off for ∼four weeks before brightening by ∼0.2 mag (Fig. 13). It is possible that once FO Aqr achieved the critical $\dot{M}$ to reestablish a viscous disk, it took longer for $\dot{M}$ to complete its recovery and replenish the disk.

It would be fruitful if a future paper were to identify concrete observational changes resulting from disk dissipation—with an emphasis on how they might be distinguished from those associated with a partially depleted accretion disk. For example, in a blob-fed geometry, we might expect to see quasi-periodic oscillations caused by beats between the WD spin and the decaying orbits of the blobs.

7.5. *Orbital waveform and eclipses*

The gradually increasing eclipse depth and width during the recovery from the 2016 low state (Figure 7) is consistent with an increase in the size of the eclipsed source. No comparable trend was present in the 2017 low-state eclipse profiles (Figure 12), possibly because the depth of that low state was significantly less than that of its 2016 counterpart.

The eclipse profiles strongly disfavor the possibility that the disk experienced a thermal transition as the system migrated between the low and high states, consistent with the lack of dwarf-nova outbursts. For example, when the accretion disk in the dwarf nova U Gem is on the cold branch, grazing eclipses of it are deep and well-defined because the stream-disk hotspot contributes a disproportionately large amount of light in comparison to the rest of the optically thin disk (Naylor & La Dous 1997). However, when the disk becomes hot and optically thick during outburst, the hotspot's relative contribution to the light curve becomes small. The eclipses shift towards earlier phases, becoming poorly defined and much shallower than in quiescence (Naylor & La Dous 1997). The absence of similar behavior in FO Aqr's eclipses as the system recovered from the low state into the bright state leads us to conclude that the disk did not undergo a thermal transition during either low state.

In light of Sec. 7.4, it is worth revisiting the assumption from Paper I that the presence of an eclipse during the 2016 low state was prima facie evidence of a disk. While the eclipse unambiguously indicates that the accretion flow encircled the WD in the orbital plane, it provides no information about the nature of the flow's velocity field, the key feature that distinguishes disk-fed and blob-fed accretion (King & Wynn 1999). Thus, the mere fact that the eclipse was present throughout the observed segments of the three low states does not necessarily mean that a Keplerian accretion disk was present.

7.6. *Flares near the beginning and end of the low states*

FO Aqr shows several photometric flares consistent with brief spurts in the accretion rate near the beginning and end of the low states. This behavior was especially conspicuous in the 2018 light curve (Fig. 13), which showed three discrete flares, each with an amplitude of ∼0.25 mag, when the system had recovered to V∼14.2. During these flares, the light curve tended to show the strong spin pulse that traditionally accompanies its high states, but between the flares, the variability in the light curve became erratic.

A flare shortly after the start of the 2017 low state on Aug. 27 suggests that this behavior might occur near the beginning of low states, too. As Fig. 11 indicates, there were two time-series observations of this flare, separated by ∼12 h. The first showed the system at $V \sim 14.0$ with a 0.5-mag spin pulsation and no significant power at either $\omega - \Omega$ or $2(\omega - \Omega)$. By the start of the second time series, FO Aqr had faded by a quarter magnitude, and its power spectrum showed signals at ω, $\omega - \Omega$, and $2(\omega - \Omega)$, suggesting a change in the mode of accretion as the system faded. This flare occurred just 31 h after we obtained the first light curve to show significant power at $2(\omega - \Omega)$ during the 2017 observing season.

The behavior of the grazing eclipse offers evidence that these were not dwarf-nova outbursts. If these flares were from a thermal instability in an accretion disk, the disk would need to be cool and optically thin outside of the flares, which in turn would cause the eclipse depth to increase because of the increased relative contribution of the stream-disk hotspot (Sec. 7.5). The decreased eclipse depth during the low states contradicts this prediction. Instead, we propose that the flares correspond with brief instances of a ring of blobs becoming a viscous disk. This would occur when the viscous timescale of the blobs becomes lower than the timescale on which they are accreted.

8. CONCLUSION

Our major findings are as follows.

- There is a fundamental link between the brightness of FO Aqr and its power spectrum. When brighter than $V \sim 14$, its light curve tends to be spin-dominated with only a minimal contribution from the beat frequency; when fainter, the amplitudes of the spin and beat frequencies become comparable.

- The mode of accretion depends strongly on the accretion rate. Only when FO Aqr dropped below $V = 14$ was there a strong, persistent interaction between the accretion stream and the WD magnetosphere. This is close to the magnitude at which Hameury & Lasota (2017) predicted that the accretion disk would dissipate.

- FO Aqr never fully recovered to its pre-2016 optical brightness, suggesting that the mass-transfer rate remained lower than its historical level. This is consistent with the finding by Kennedy et al. (2017) that FO Aqr's X-ray luminosity remained unusually low after the end of the 2016 low state.

- The eclipse was present in phase-averaged orbital profiles throughout all three states, meaning that a disk-like structure was present at all times during our observations. It is unclear from the eclipses whether this structure was a viscous, Keplerian accretion disk or a ring of diamagnetic blobs.

- Our observations are consistent with the proposal by Hameury & Lasota (2017) that the accretion disk dissipated and was replaced by a ring of diamagnetic blobs, but a future theoretical study will need to identify specific observational characteristics of the diamagnetic-blob model that unambiguously distinguish it from stream-overflow accretion.

- The observations from 2016 and 2018 include a pair of transitions from a low state into a high state. In both instances, FO Aqr's light curve stabilized into a bright state after going through a series of erratic, low-amplitude flares on timescales of days. This behavior was particularly well-observed in 2018.

- The 2017 low state began in earnest with a ∼two-week-long decline, after which the light curve showed a ∼0.4-mag drop into the low state. This drop corresponded with an immediate transition from a spin-dominated light curve to beat-dominated.

- Our spin ephemeris links all pulse timings obtained since 2002 and establishes that the recent fusillade of low states began shortly after the WD reverted to a spin-down state in 2014.

- The X-ray spectrum of FO Aqr during the 2017 high state was unchanged from the 2016 high state. In both epochs, the spectrum had a significant excess of soft X-rays. The disappearance of the soft X-rays before the optical eclipse is consistent with photoelectric absorption by vertically extended disk structure.

- Digitized photographic plates from APPLAUSE reveal that FO Aqr experienced previously unknown low states in 1965, 1966, and 1974. There are no measurements of $\dot{P}$ during those years, but if the duration of a typical spin-down episode is approximately equal to the duration of the 1988-2014 spin-up, these low states would have occurred when the WD was spinning down.

ACKNOWLEDGMENTS

This work has made use of data from the European Space Agency (ESA) mission *Gaia* (https://www.cosmos.esa.int/gaia), processed by the *Gaia* Data Processing and Analysis Consortium (DPAC, https://www.cosmos.esa.int/web/gaia/dpac/consortium). Funding for the DPAC has been provided by national institutions, in particular the institutions participating in the *Gaia* Multilateral Agreement. MRK is supported by a Newton International Fellowship provided by the Royal Society. We would like to thank Norbert Schartel and the *XMM-Newton* OTAC for granting us ToO observations of FO Aqr in 2017.

The Center for Backyard Astrophysics is supported in part by NSF award AST-1615456.

Funding for APPLAUSE has been provided by DFG (German Research Foundation, Grant), Leibniz Institute for Astrophysics Potsdam (AIP), Dr. Remeis Sternwarte Bamberg (University Nuernberg/Erlangen), the Hamburger Sternwarte (University of Hamburg) and Tartu Observatory. Plate material also has been made available from Th uringer Landessternwarte Tautenburg.

Software: Astropy (Astropy Collaboration et al. 2013, 2018)

Facilities: AAVSO, Gaia, Kepler, XMM

REFERENCES

Astropy Collaboration, Robitaille, T. P., Tollerud, E. J., et al. 2013, A&A, 558, A33.

Astropy Collaboration, Price-Whelan, A. M., Sipócz, B. M., et al. 2018, AJ, 156, 123.

Augusteijn, T. 1990, IAU Colloq. 122: Physics of Classical Novae, 50.

Andronov, I. L., Ostrova, N. I., & Burwitz, V. 2005, The Light-time Effect in Astrophysics: Causes and Cures of the O-C Diagram, 229.

Bailer-Jones, C. A. L., Rybizki, J., Fouesneau, M., et al. 2018, AJ, 156, 58.

Beardmore, A. P., Mukai, K., Norton, A. J., et al. 1998, MNRAS, 297, 337.

Bernardini, F., de Martino, D., Mukai, K., et al. 2019, MNRAS, 484, 101.

Bonnardeau, M. 2016, IBVS, 6181, 1.

de Martino, D., Buckley, D. A. H., Mouchet, M., et al. 1994, A&A, 284, 125.

Drake, A. J., Djorgovski, S. G., Mahabal, A., et al. 2009, ApJ, 696, 870.

Evans, P. A., Hellier, C., Ramsay, G., et al. 2004, MNRAS, 349, 715.

Ferrario, L. & Wickramasinghe, D. T. 1999, MNRAS, 309, 517.

Gaia Collaboration, Prusti, T., de Bruijne, J. H. J., et al. 2016, A&A, 595, A1.

Gaia Collaboration, Brown, A. G. A., Vallenari, A., et al. 2018, A&A, 616, A1.

Garnavich, P. & Szkody, P. 1988, PASP, 100, 1522.

Hameury, J.-M., & Lasota, J.-P. 2017, A&A, 606, A7.

Hellier, C. 1993, MNRAS, 265, L35.

Hellier, C. & Beardmore, A. P. 2002, MNRAS, 331, 407.

Hellier, C., Mason, K. O., & Cropper, M. 1989, MNRAS, 237, 39P.

Kennedy, M. R., Garnavich, P., Breedt, E., et al. 2016, MNRAS, 459, 3622.

Kennedy, M. R., Garnavich, P. M., Littlefield, C., et al. 2017, MNRAS, 469, 956.

King, A. R., & Lasota, J.-P. 1991, ApJ, 378, 674.

King, A. R. & Wynn, G. A. 1999, MNRAS, 310, 203.

Kochanek, C. S., Shappee, B. J., Stanek, K. Z., et al. 2017, PASP, 129, 104502.

Kunze, S., Speith, R. & Hessman, F. V. 2001, MNRAS, 322, 499.

Littlefield, C., Garnavich, P., Kennedy, M. R., et al. 2016, ApJ, 833, 93.

Littlefield, C., Myers, G., Sabo, R., Garnavich, P., & Kennedy, M. 2017, ATel, 10703, 1.

Littlefield, C., Stiller, R., Hambsch, F.-J., et al. 2018, The Astronomer's Telegram, 11844, 1.

Livio, M., & Pringle, J. E. 1994, ApJ, 427, 956.

Marsh, T. R., & Duck, S. R. 1996, NewA, 1, 97.

Marshall, F. E., Boldt, E. A., Holt, S. S., et al. 1979, ApJS, 40, 657.

Marsh, T. R., Gänsicke, B. T., Hümmerich, S., et al. 2016, Nature, 537, 374.

Mason, K. O., Breeveld, A., Much, R., et al. 2001, A&A, 365, L36.

Murray, J. R., Armitage, P. J., Ferrario, L., et al. 1999, MNRAS, 302, 189.

Naylor, T. & La Dous, C. 1997, MNRAS, 290, 160.

Norton, A. J., Wynn, G. A., & Somerscales, R. V. 2004, ApJ, 614, 349.

Osborne, J. P., & Mukai, K. 1989, MNRAS, 238, 1233.

Pakull, M. W., & Beuermann, K. 1987, Ap&SS, 131, 641.

Patterson, J. 1994, PASP, 106, 209.

Patterson, J. 2012, JAAVSO, 40, 240.

Patterson, J., & Steiner, J. E. 1983, ApJL, 264, L61.

Patterson, J., Kemp, J., Richman, H. R., et al. 1998, PASP, 110, 415.

Shafter, A. W., & Targan, D. M. 1982, AJ, 87, 655.

Shafter, A. W., & Macry, J. D. 1987, MNRAS, 228, 193.

Shappee, B. J., Prieto, J. L., Grupe, D., et al. 2014, ApJ, 788, 48.

Strüder, L., Briel, U., Dennerl, K., et al. 2001, A&A, 365, L18.

Steiman-Cameron, T. Y., Imamura, J. N., & Steiman-Cameron, D. V. 1989, ApJ, 339, 434.

Turner, M. J. L., Abbey, A., Arnaud, M., et al. 2001, A&A, 365, L27.

Waagen, E. O. 2016, AAVSO Alert Notice, 545.

Waagen, E. O. 2017, AAVSO Alert Notice, 598.

Waagen, E. O. 2018, AAVSO Alert Notice, 644.

Warner, B. 1986, MNRAS, 219, 347.

Warner, B. 1988, Nature, 336, 129.

Warner, B. 1990, Ap&SS, 164, 79.

Warner, B., & Wickramasinghe, D. T. 1991, MNRAS, 248, 370.

Williams, G. 2003, PASP, 115, 618.